Fall 2010

Calcium carbonate precipitation mechanisms and geochemical analysis of particulate material found within the waters of Maramec Spring, St. James, Missouri

Kyle Steven Rybacki

CALCIUM CARBONATE PRECIPTATION MECHANISMS AND GEOCHEMICAL ANALYSIS OF PARTICULATE MATERIAL FOUND WITHIN THE WATERS OF MARAMEC SPRING, ST. JAMES, MISSOURI

by

KYLE STEVEN RYBACKI

A THESIS

Presented to the Faculty of the Graduate School of the

MISSOURI UNIVERSITY OF SCIENCE AND TECHNOLOGY

In Partial Fulfillment of the Requirements for the Degree

MASTER OF SCIENCE IN GEOLOGY & GEOPHYSICS

2010

Approved by

David Wronkiewicz, Advisor
Francisca Oboh-Ikuenobe
Wan Yang

ABSTRACT

The purpose of the present study is to determine whether a mineral phase is precipitating from solution in the natural Maramec Spring system giving the spring water a milky blue color, to identify the mineral phase, and to investigate potential mechanisms for inducing precipitation. Maramec Spring is a first-order magnitude spring located 11 km southeast of St. James, Missouri.

The water that expels from Maramec Spring varies between being near saturation, but undersaturated in calcium, with respect to calcite (saturation index of 0.994 mg/L). Moving downstream, away from the conduit, the spring waters increase in pH and temperature. Eh is observed to decrease, in response to increasing pH. Conductivity, calcium, magnesium, and total hardness, as well as alkalinity were measured to be constant along the entire stream reach. Conductivity tends to be higher on sampling dates following local rainfall events. A positive CO_2 flux, greatest at the point of upwelling, is observed at the spring.

At this time the particulate material which is responsible for giving Missouri spring waters their milky blue color cannot be positively identified. Spring water chemistry favors calcium carbonate precipitation through CO_2 degassing, but vacuum filtration suggests calcite is not a major phase. The milky blue color of the spring water is hypothesized to be a combination of calcium carbonate, or suspended colloidal quartz and clay minerals (kaolinite, smectite, or chlorite) from deeper within the spring conduit.

ACKNOWLEDGMENTS

First, I would like to thank my advisor Dr. David Wronkiewicz for his patience and guidance. Because of him I am a better scientist, and have greatly refined my taste in beer. Secondly, I would like to thank my committee members, Drs. Oboh-Ikuenobe and Yang, for their considerate revisions which greatly improved the quality of this thesis. I would also like to thank the James Foundation, Maramec Spring Park, the Department of Energy Grant (DE-FE0002416, "Geoscience Perspectives in Carbon Sequestration – Educational Training and Research through Classroom, Field, and Laboratory Investigations") and the opportunities for Undergraduate Research Experience (OURE) program of Missouri University of Science and Technology for funding. Since this project would have been impossible to complete by myself I would like to extend thanks to: Dr. F. Scott Miller, Dr. Nathan Miller, Eric Bohannan, Carrie Bender, the 2007 Aqueous Geochemistry/Environmental Aquatic Chemistry class, Jeffrey "Spike" Crews, and Sarah Null for their assistance with laboratory and field work. Finally, I would like to thank my family. If it was not for their love and support through the years, I would have never realized my full potential. All that I am today is because of them.

TABLE OF CONTENTS

LIST OF ILLUSTRATIONS

Page

LIST OF TABLES

1. INTRODUCTION

The water emanating from many Missouri springs is relatively clear under normal flow conditions, but generally retains a milky blue color due to the presence of fine-grained colloidal particles. The milky blue color is present under all seasonal conditions except during flood stages when particulate materials suspended in the water column impart a brownish color and increase water turbidity. The waters of Missouri springs can be undersaturated to supersaturated in calcium and magnesium with respect to calcite and dolomite. The calcium and magnesium are derived from the dissolution of carbonate strata in the spring recharge area. To the authors' knowledge, no studies have ever been conducted to identify the precipitate material in this or other springs in southeastern Missouri.

Maramec Spring is Missouri's fifth largest cold-water spring. It is located in Phelps County, Missouri, 11 km southeast of St. James. The spring expels, on average, approximately 3.6×10^8 liters of water/day (9.6×10^7 gallons/day) from a large open conduit hosted in the Ordovician dolomite of the Gasconade Formation. The recharge area of the spring is estimated to encompass 800 square kilometers to the south and west (Unklesbay and Vineyard, 1992; Vandike, 1996). The spring conduit has been mapped by scuba divers over a distance of approximately 940 meters, and a maximum depth of approximately 61 meters, but this survey conducted by the divers included only a minuscule portion of the cave system.

The Gasconade Formation hosts many well developed karst features (e.g., caves, springs, etc.) across central and southern Missouri, including Maramec Spring (Orndorff et al., 2006). The Gasconade Dolomite is on average 100 meters thick, varies in color from gray to buff, is finely to coarsely crystalline, moderately to thickly bedded, and contains one prominent sandstone bed, the Gunter Sandstone Member (Thompson, 1991). The Gasconade is unofficially broken into the "lower Gasconade" and "upper Gasconade." The lithologic feature for this distinction is the abundance of chert within the "lower Gasconade," while the "upper Gasconade" is relatively chert free. The basal sandstone bed of the Gasconade is classified as the Gunter Sandstone Member and occurs along the base of this unit and marks the contact between the Eminence (Cambrian) and

Gasconade (Ordovician) Formations. The Gunter Sandstone is on average 10 meters thick, varies in color from white to reddish-brown, is medium grained, and is thinly bedded with some minor cross-bedding. It is generally a quartz sandstone, but in some places the Gunter is described as a sandy dolomite. This sandstone is a major aquifer for municipal wells throughout Missouri and most likely the major conduit for waters expelling from Maramec Spring.

1.1. PREVIOUS STUDIES

The hydrology of Maramec Spring has been extensively studied by various researchers. For a complete discussion on the hydrology of Maramec Spring refer to Vandike (1996) and the references cited therein. Most of the studies in the literature were in response to a liquid fertilizer pipeline break that affected the spring in November of 1981. They examined water quality, and evaluating hydrologic modeling (Vandike, 1985, 1996; Wicks and Hoke, 2000).

Calcium carbonate precipitation kinetics is of great importance to scientists and engineers. Precipitation mechanisms need to be well understood in order to minimize problems of scale buildup in residential and industrial settings. Calcium carbonate precipitation from supersaturated solutions is known to reduce the permeability and porosity in reservoir rocks, the efficiency of water softening devices, and clog the piping of residential and commercial water systems utilizing hard water.

1.1.1. Conductivity, pH, pCO_2, and [Ca^{+2}]. The [Ca^{+2}] in solution (Dove and Hochella, 1993), CO_2 loss (Dreybrodt et al., 1997; Zhang and Grattoni, 1998), and pH (Wilson, 1975) are considered to be the three dominant factors influencing calcium carbonate precipitation. Groundwater usually contains dissolved CO_2 contents 10 to 100 times greater than atmospheric levels, especially in carbonate strata (Lebron and Suarez, 1996). A decrease in solution pH is observed during the experimental crystallization of calcium carbonate. This pH change is attributed to the loss of CO_2 from the system (Reddy and Nancollas, 1971; Lakshtanov and Stipp, 2010). Theoretically, one mole of CO_2 should be released for every mole of calcium carbonate precipitated (Zhang and

Grattoni, 1998). Since pH can easily be measured *in situ*, many scientists use pH as a proxy to estimate for the amount of calcium carbonate precipitated from solution.

Several studies propose that the degree of calcium saturation in solution, with respect to calcite, is the dominant factor influencing calcium carbonate crystallization in aqueous systems (Kamkha et al., 1989; Dove and Hochella, 1993; Gómez-Morales et al., 1996; Teng et al., 2000; Dickinson et al., 2002; Lakshtanov and Stipp, 2010). In this scenario conductivity can be used as a proxy, in addition to pH, to measure the relative change in [Ca^{+2}] over time. Gómez-Morales et al. (1996) were able to measure induction times using pH and [Ca^{+2}], but found that [Ca^{+2}] was not as sensitive an indicator to the induction of calcite crystallization as was pH.

1.1.2. Calcium Carbonate Polymorphs and Crystal Forms. Laboratory crystallization experiments can produce all three polymorphs of calcium carbonate (i.e. calcite, aragonite, and vaterite). However, the most commonly occurring polymorph is calcite (Reddy and Nancollas, 1976). Swinney et al. (1982) experimentally determined that hard waters are softened more efficiently by the precipitation of rhombohedral calcite rather than aragonite; vaterite was never observed. This is attributed to the variation in crystal habit between calcite and aragonite, i.e. the aragonite crystals take up more space reducing the efficiency of the water softener. Vaterite was only observed precipitating in unseeded supersaturated solutions where concentrations were extremely high (Gómez-Morales et al., 1996).

Not only are the rates of precipitation of all the polymorphs of calcium carbonate important, but so are the transformation rates from one polymorph to another. Polymorphic transformations are believed to occur by the dissolution of the parent phase(s), aragonite or vaterite, and the growth of the more stable phase, calcite (Ogino et al., 1990). Calcite growth is also believed to be the rate limiting step in polymorphic transformation, and not the dissolution of the less stable polymorph. Transformation rates between all polymorphs are slowed in the presence of Li^{+}.

1.1.3. Calcium Carbonate Crystal Growth. The growth of calcium carbonate crystals from solution is predominantly studied in one of two ways. The first and most common way is with the addition of calcite seed crystals, which act as nucleation sites for the calcium carbonate crystallization from supersaturated solutions. The second, but

much less common method is the spontaneous nucleation of calcium carbonate from supersaturated solutions in the absence of seed crystals. The calcium carbonate precipitation mechanics appear to be the same for seeded crystallization experiments as they are for spontaneous nucleation experiments. Spontaneous nucleation occurs almost instantaneously and is not ideal for studying the ***rates*** of calcium carbonate precipitation since extremely high saturation indices are necessary to initiate spontaneous nucleation. Spontaneous nucleation of calcium carbonate is ideal for estimating the ***amount*** of calcium carbonate precipitated from solution since there is no crystalline material prior to induced crystallization. For these reasons the spontaneous nucleation method of precipitating calcium carbonate will not be discussed any further. Seed crystals are usually euhedral, transparent, approximately 10μm in size (Reddy and Nancollas, 1971), and retain their euhedral shapes throughout calcium carbonate growth (Goodarz-nia and Motamedi, 1980).

Several authors propose that calcium carbonate precipitation in a seeded experiment is surface area controlled (Reddy and Nancollas 1971; Nancollas and Reddy 1971; Reddy and Gillard, 1981; Ogino et al., 1990; Dove and Hochella, 1993). The growth rate of calcite is believed to be proportional to the number of available growth sites, thus making the process controlled by crystal surface area (Ogino et al., 1990). This surface area controlled process may be the rate limiting step for calcite crystal growth (Nancollas and Reddy, 1971; Zhang and Grattoni, 1998). Calcite growth is proposed to occur in a stepwise (Reddy and Gillard, 1980) or spiral fashion (Dove and Hochella, 1993).

1.1.4. Calcium Carbonate Precipitation in the Presence of Contaminants. The effect of natural contaminants (e.g., Mg, Mn, Sr, Si, SO_4^{-2}, PO_4^{-3}, and dissolved organic carbon) on the precipitation of calcium carbonate is of great industrial importance. Of these natural contaminants, Mg (Reddy and Nancollas, 1976), Si (Lakshtanov and Stipp, 2010), PO_4^{-3} (Reddy and Nancollas, 1973, Nancollas, 1979), and dissolved organic carbon (DOC) (Lebron and Suarez, 1996) all have a dramatic effects on the rate of calcium carbonate precipitation. DOC and PO_4 affect crystal growth by attaching to and reducing the number of potential precipitation sites on crystal surfaces (Reddy and Nancollas, 1973; Dove and Hochella, 1993; Lebron and Suarez, 1996).

Some studies propose that the formation of an amorphous phase of calcium carbonate occurs prior to crystallization in the presence of certain contaminants (Reddy and Nancollas, 1976; Söhnel and Mullin, 1982). In the presence of PO_4, amorphous shapes and jagged edges were common during calcite growth (Dove and Hochella, 1993). The crystalline calcite precipitated from supersaturated solutions with Mg present was preceded by an amorphous calcium carbonate phase and then conversion to a crystalline form similar to calcite crystals observed to grow in the absence of Mg. The size of the calcite crystals also appear to be correlated to the amount of impurities incorporated within the calcite crystal structure, i.e. more impurities yielded smaller crystals (Söhnel and Mullin, 1982).

Gebauer et al. (2008) also observed an amorphous phase that preceded the crystalline phase. They proposed the growth of stable calcium carbonate clusters through the binding of ions. Ca^{+2} and CO_3^{-} ions bind together to form an amorphous phase without any crystalline structure. These non-crystalline clusters then convert into the most thermodynamically stable calcium carbonate polymorph. All steps associated with ion binding are anticipated to be pH dependent.

Contaminants are also observed to affect the polymorph of calcium carbonate precipitated from supersaturated solutions, the crystallization induction rate, as well as the polymorphic transformation rate. The presence of silica appears to have an effect on the calcium carbonate polymorph precipitate and the rate of induction (Lakshtanov and Stipp, 2010).

1.1.5. Calcium Carbonate Reaction Rates. The exact role of kinetics and thermodynamics in calcium carbonate precipitation is not well understood. In calcite precipitation there is an initial rapid growth surge of calcium carbonate that eventually slows to follow kinetic rate equations for the precipitation of calcium carbonate (Nancollas and Reddy, 1971). The most commonly proposed rate limiting steps are CO_2 production (Dreybrodt et al., 1997; Zhang and Grattoni, 1998), the number of available growth sites (Dove and Hochella, 1993; Zhang and Grattoni, 1998), system flow characteristics (Dreybrodt et al., 1997), and $[Ca^{+2}]$ saturation levels (Dove and Hochella, 1993).

Most researchers are in agreement that the most important thermodynamic factor is the [Ca^{+2}] in solution, but the most important kinetic factor is still debatable. For example, Kamkha et al. (1989) and Dickinson et al. (2002) had differing views about kinetic factors. Kamkha et al. (1989) suggested that pH, specifically the [HCO_3^-], controlled the kinetics of calcium carbonate precipitation, but Dickinson et al. (2002) proposes that the kinetics of the growth reactions were controlled by CO_2 release. The genetic linkage between CO_2 release and [HCO_3^-] suggests that both authors may be correct.

The [Ca^{+2}] in solution intuitively is the most plausible kinetic factor affecting calcium carbonate crystallization. Varying the [Ca^{+2}] relative to the saturation level within a system has a profound effect on growth rates and mechanisms of calcium carbonate. In solutions with saturation levels greater than 1 but less than 2, calcite exhibits two different types of growth. First, calcite growth is dominated by surface nucleation and coalescence, but transitions to a mechanism resembling spiral growth over time. In undersaturated solutions, which are close to equilibrium, both surface dissolution and precipitation of calcium carbonate appear to occur simultaneously (Dove and Hochella, 1993).

Theoretically, one mole of CO_2 is produced for every mole of calcium carbonate precipitated. Thus, the rate at which CO_2 can be produced and removed from the system can also be a rate limiting step for calcium carbonate precipitation. In natural settings aquatic organisms may have a positive effect on the rate of calcium carbonate precipitation as they consume CO_2 for vital processes (Lebron and Suarez, 1996). Dreybrodt et al. (1997) studied the effect of enzymes on the $HCO_3^- + H^+ \rightarrow H_2O + CO_2$ reaction rate to determine if CO_2 production could be enhanced. They observed that this reaction was enhanced in the presence of the enzymes, suggesting a linkage of CO_2 removal and carbonate precipitation. The exact role the enzymes play is not well understood (Zhang and Grattoni, 1998).

In the simplest of systems one parameter may act as the rate limiting step in calcium carbonate precipitation. In more complex systems, such as a natural system, many parameters may affect the rate at which calcium carbonate is precipitated from solution. For example, in turbulent flow systems concentration gradients have a limited

ability to form, thereby homogenizing the surface fluid chemistry near the crystal surface and directly affecting the calcium carbonate precipitation rate. To further complicate issues, some studies observed a quasi-equilibrium phase prior to true chemical equilibrium. The quasi-equilibrium is represented in the data as a change in slope of the concave parabolic curve of $[Ca^{+2}]$ in solution. Initially, $[Ca^{+2}]$ in solution decreases very rapidly, but slows over time. The quasi-equilibrium is maintained for a substantial period of time until the system reaches true chemical equilibrium (Dreybrodt et al., 1997).

When comparing all these studies, it becomes apparent that calcium carbonate precipitation rate laws need to be carefully selected and applied (Teng et al., 2000). Analyzing the change in bulk chemistry of a system may not be the most accurate way to derive rate laws of calcium carbonate precipitation (i.e. discrepancies between rate law equations from studies of different scales). For example, Goodarz-nia and Motamedi (1979) observed an interesting phenomenon during their experimental precipitation of calcium carbonate that was not noted in any other study. When precipitating calcium carbonate, they observed that the overall crystal size increased with time until approximately 50 minutes after initial precipitation. After this time, the crystal sizes were observed to decrease, rather than continuing to grow. They could not explain this phenomenon, which could have been the result of the system reaching equilibrium, achieving slightly undersaturated conditions, or transformation from one polymorphous phase to another with lower equilibrium solubility values.

1.1.6. Calcium (^{45}Ca) Isotope Exchange. Using a calcium (^{45}Ca) radiotracer, calcium isotope exchange between seed crystals and solution was measured (Reddy and Nancollas, 1971). Calcium isotope exchange between seed crystals and solution is dependant upon the saturation of solution with respect to Ca. For example, in a saturated solution isotope exchange occurs between the seed crystal and solution, but very little exchange occurs during the first hour of crystallization. In contrast, Ca isotope exchange does not take place in supersaturated solution (i.e. calcite is precipitated in isotopic equilibrium with the solution).

1.2. STUDY OBJECTIVES

The purpose of the present study is to: (1) determine whether a mineral phase is precipitating from solution in the natural Maramec Spring system to give the spring water its milky blue color; (2) identify the mineral phase; and (3) investigate potential mechanisms for inducing precipitation (Figure 1.1). In today's society, calcium carbonate precipitation and dissolution processes are of the extreme importance with respect to CO_2 sequestration. A good understanding of carbonate system behavior under varying natural conditions is necessary to enhance CO_2 sequestration attempts. Natural analogs such as Maramec Spring and the Bahamian Platform act as natural laboratories to study carbonate precipitation and dissolution (i.e. sedimentation and karstification), which can then be applied to CO_2 sequestration studies.

Figure 1.1. Photograph of Maramec Spring from sampling location 3 looking towards sampling location 1. The swell of the spring is located in the top left-center portion of the photograph just below the base of the rock wall. Note the milky blue color of the Maramec Spring water in the pool.

2. EXPERIMENTAL METHODS

2.1. FIELD SAMPLE LOCATIONS AND SITE LOCATIONS

The Maramec Spring branch is approximately 1,400 meters in length from its point of initial upwelling from the subsurface to its termination where it merges with the Meramec River (Figure 2.1). The spring branch flows from south to north. The stream originates at the spring swell (sampling location 1) and is comprised of a series of rapids (sampling locations 3, 6, 7, and 8), shallow riffles (location 4), slow moving water pools (locations 2; Figure 1.1), and deeper (>2 meters), slower moving pools (locations 5) (Table 2.1).

Field measurements were collected by experienced and supervised inexperienced personnel. Experienced data collectors included undergraduate geology students, geology graduate students and geology faculty. Inexperienced data collectors included high school summer camp students and undergraduate students from other disciplines. All inexperienced data collectors were supervised by experienced data collectors. The data collected by the inexperienced personnel is valid, but not as precise as the data collected by experienced personnel.

The first eight trips to the site from 2002 and 2007 were in association with the Jackling summer camp for high school student hosted by Missouri University of Science and Technology each summer. The eight sampling locations were selected to analyze the water chemistry of Maramec Spring (Figure 2.1). Spring water chemical data and lab samples were collected over 12 sampling trips during the summer months from 2007 to 2010 (Table 2.2). Not all eight locations were sampled on each trip because of time restrictions imposed by the detailed sampling process. Water pH and Eh measurements from these earlier trips are referenced in the present study, although used with caution given the inexperience of the various student samplers.

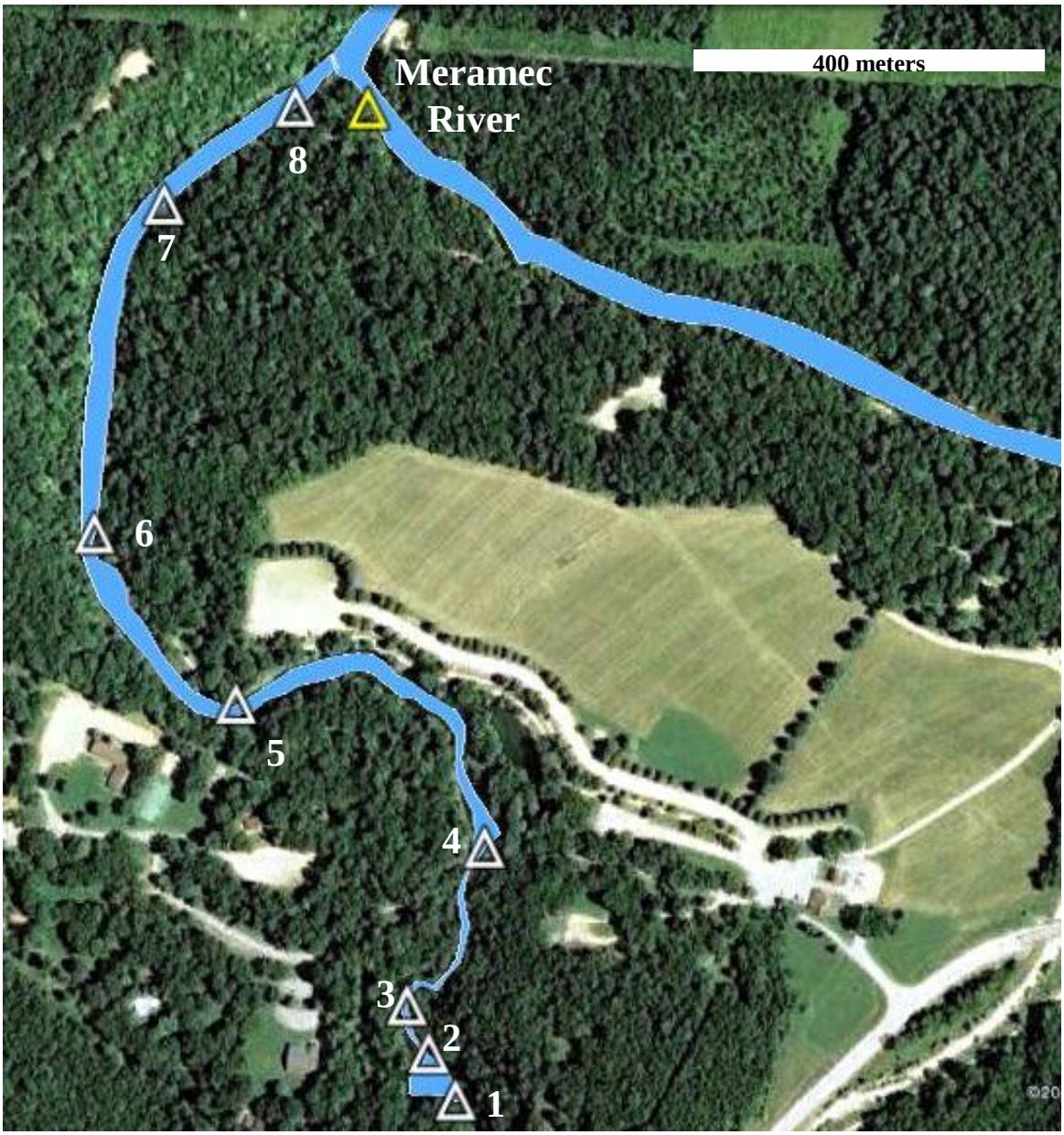

Figure 2.1. Aerial photograph outlining the sampling locations at Maramec Spring utilized in this study, 11 km southeast of St. James, Missouri. The spring conduit is located at sampling location 1. Stream flow is from south (bottom of photograph) to north (top of photograph). The roadway in the lower right corner of the photograph is Missouri Highway 8.

Table 2.1. Maramec Spring sampling locations and their respective distances from conduit, and flow characteristics

Sampling Location	Distance Downstream	Location/Stream Characteristics
1	0 m	Conduit; variable flow depending upon amount of rainfall
2	55 m	Steady flow, 0.5 m deep water along flank of deeper pool
3	85 m	First rapids below conduit and pool
4	285 m	Next to steps below bridge on the oppsite side of the sidewalk, shallow water (~15 cm)
5	670 m	Across from deep water sign, slow moving water, > 2 m deep, lots of aquatic plants
6	800 m	Rapids, just below outhouse
7	1200 m	Rapids
8	1300 m	Rapids, just after suspension bridge
Meramec River		75 m East of sampling location 8; much slower flow rates than spring arm

Table 2.2. Maramec Spring sampling information including personnel, locations sampled, relative flow conditions, and weather. Jackling = Jackling Introduction to Engineering summer camp participants; GEO 376/Env. Eng 261 = Aqueous Geochemistry/Environmental Aquatic Chemistry Class.

Date	Help	Locations Sampled	Flow Conditions	Weather Prior to Sampling
6/14/2001	Jacking	1,2,3,4		Rain night before
6/13/2002	Jacking	1,2,3,4		Rain night before
6/20/2002	Jacking	1,2,3,4		No rain for week
6/28/2002	Jacking	1,2,3,4,5		Light rain
6/12/2003	Jacking	1,2,3,4,5	High discharge	Heavy rain
6/20/2003	Jacking	1,2,3,4,5	Slightly higher discharge	Light rain
6/27/2003	Jacking	1,2,3,4,5		Heavy rain day before
7/10/2007		1,2,3,4,5	Normal discharge	No rain
9/21/2007		1,2,3,4,5,6,7,8	Normal discharge	No rain
10/4/2007	GEO 376/ Env. Eng 261	1,2,3,4,5,6,7,8		
3/12/2008		1,2,3,4,5,6,7,8		
8/29/2010		1,2,3,4,5,6,7,8	Normal discharge	No rain
10/6/2010		1,2,3,4,5,6,7,8	Normal discharge	No rain

2.2. FIELD MEASUREMENTS

Measurements collected *in situ* include: temperature, pH, Eh, conductivity, and dissolved oxygen. Calcium hardness, total hardness, and alkalinity were measured *ex situ* on site using portable Hach field titration kits. Turbidity measurements (i.e, the scattering of light within a water sample) were attempted on several occasions, but the constant high humidity of the spring area combined with the cool water temperatures

induced condensation on the sample vial. For these reasons turbidity was only accurately measured on the March 12, 2008 sampling.

All instruments utilizing standards (e.g., pH and conductivity probes) were calibrated with their respective commercial laboratory standards prior to use. In the field all instruments were continually checked to measure the amount of instrument drift, and re-calibrated if instrument drift exceeded preset parameters (Appendix A).

Temperature, pH, and Eh were all measured using a Fisher Scientific Accumet AP115 portable pH/ORP meter. Temperature, pH, and Eh measurements have a factory accuracy of ±0.3°C, ±0.1, and ±2 mV, respectively. The pH probe was calibrated using factory pH standards of 4.00 ± .01, 7.00 ± .01, and 10.00 ± .01. Temperature, pH, and Eh were measured at all eight sampling locations, but not at every location on every sample trip.

Conductivity was measured using a WTW Cond 330i/SET portable conductivity meter. The conductivity meter was calibrated using commercial standards of 100.6, 398.7, and 1002 μSiemens/cm. The conductivity meter, which has a factory accuracy of ±0.1 μSiemens/cm, did not drift (i.e., the 100.6 standard read 100.6 after all measurements) after calibration. Conductivity measurements were conducted at all eight sampling locations, but not on all sampling trips.

Dissolved oxygen (DO) was measured using a Fisher Scientific Accumet AP64 portable dissolved oxygen meter with an Au/Ag cathode/electrode. The DO probe a reporting accuracy 0.12 mg/L with a precision of ±0.02 mg/L. It was calibrated by saturating a sponge with de-ionized water and allowing it to equilibrate in a 100% relative humidity environment. No drift was observed within the DO probe from location to location. The DO measurements were collected at all eight sampling locations on the last round of sampling. To test the accuracy of the measurements the DO probe was immersed in a CO_2 rich/O_2 poor atmosphere. It reported less than 0.12 mg/l of dissolved oxygen in this environment.

Turbidity and CO_2 flux measurements were each only collected during one trip. Turbidity was measured using a HACH 2100P Turbidimeter. The turbidity meter was calibrated using Gelex standard of 6.11 NTU with an accuracy of ± 0.04 NTU. These CO_2 flux measurements are not referenced to a standard.

Alkalinity, calcium, and total hardness were measured on site using Hach Colorometric titration kits. All titrations were completed following the procedures distributed with each kit. Magnesium hardness was calculated by subtracting the measured calcium hardness from the total measured hardness. Alkalinity, calcium, and total hardness data were only collected at the first four sampling locations and only measured on unfiltered water samples during the last three sampling trips. On one sampling expedition (October 4, 2007), the total hardness, calcium hardness, and alkalinity were measured using unfiltered water at sampling locations 1 through 5. This detailed sampling was only completed once.

2.3. SOLUTION ANALYSES

The spring water was collected for geochemical analysis on one sample trip. Filtered water samples were collected using a disposable 60 mL sterile syringe and 5 μm nylon, 0.45 μm cellulose acetate, and 0.02 μm alumina Whatman filters at locations 1, 2, 3, and 4. These unfiltered and filtered water samples were acidified using ultra-pure HNO_3 to a pH of 2. These acidified samples were then analyzed on a inductively coupled plasma – optical emission spectrometer (ICP-OES) to determine the spring water chemistry. Unfiltered and filtered spring water samples, approximately 120 mL each, collected from the first four sampling locations were acidified with 1 mL of high purity HNO_3 to a pH of two or lower prior to analysis. All resulting solutions were analyzed for Ca, Mg, K, Na, Si, Al, Fe, and Mn.

Spring water collected only at sampling location 1 was filtered using Millipore cellulose filters to collect and examine the particulate material on two sampling dates. On August 29th, 2010 a four liter water sample was filtered on site using a 0.22 μm cellulose filter and a mechanical vacuum filtration system. On October 6, 2010, a liter of water at sampling location 1 was filtered sequentially using 5.0 μm, 0.45 μm, 0.22 μm, and 0.05 μm cellulosic filters using the vacuum filtration system. These filters were returned to the Missouri S&T campus and examined using a scanning electron microscope (SEM) with energy dispersive spectroscopy (EDS) system.

Also on October 6, 2010, a liter of unfiltered spring water was collected at sample location 1 for total dissolved solids (TDS) and total suspended solids (TSS) analysis. TDS and TSS analyses were completed using a 0.45 μm cellulose filter and vacuum filtration. The filter was dried at 103°C for 1 hour and then weighed using a precision four decimal place balance. The filter was pre-wetted and placed on a pre-cleaned filter apparatus for filtration. After filtration, the filter paper was removed from the apparatus, covered, and allowed to dry at room temperature. After drying the filter paper was further dried in a 103°C oven for 1 hour. TSS was calculated by subtracting the difference in the weight of the filter paper. This difference is then divided by the known volume of water sample passed through the filter. The filtrate was then placed in a pre-weighed 150 mL beaker, covered with a watch glass, and placed in an oven at 90°C until the sample evaporated. The beaker was allowed to cool at room temperature for 45 minutes, and then was weighed on a four decimal place balance. TDS was calculated by subtracting the difference in the weight of the 150 mL beaker and then dividing the difference by the known volume of sample evaporated.

2.4. PARTICULATE ANALYSES

2.4.1. Scanning Electron Microscopy. Particulate material collected by centrifuging and filtering the spring water was examined by using reflected light microscopy and scanning electron microscopy (SEM) analysis. SEM analysis is one of the most important techniques that allowed us to visually examine the colloidal material present in Maramec Spring and determine their bulk composition. SEM analysis was conducted on a Hitachi S-570 with a LaB_6 filament, an accelerating voltage of 15 kV, and a working distance of 15 mm under vacuum. For energy dispersive spectroscopy (EDS) the working distance was increased to 20 mm and all other parameters were unaltered.

Samples used for SEM analysis were collected and prepared in multiple ways. At the beginning of the study 32 liters of spring water was collected in the field, brought back to the laboratory, centrifuged and decanted until enough particulate material was collected for petrographical and geochemical analyses. The crystals accumulated by the centrifuge technique were selected by hand using a Nikon binocular microscope and

stainless steel probe. This material was then mounted on an aluminum SEM stub using a carbon mounting adhesive. Other SEM samples were prepared by pipetting a small aliquot of centrifuged material onto a glass slide and allowing the remaining water to evaporate prior to being mounted on a round aluminum stub. Other samples were carbon coated and examined on the SEM.

Collecting water samples in the field and returning them back to the laboratory for centrifugation was not considered to be an ideal sampling protocol because degassing of CO_2 from the water might induce chemical changes in the water (e.g., a pH increase) that could lead to additional precipitation or digestion reactions. Filtration techniques were therefore employed to collect the particulate material present in the Maramec Spring water solution directly in the field. For this analysis four liters of water was filtered on site *ex situ* using a 0.22 μm cellulose filter. The filter and collected particulate material were mounted on an aluminum stub and coated with Au + Pd for 120 seconds at 10 mAmps. A "blank" sterile filter sample was also prepared for analysis on the SEM to help distinguish particulate material from the filter substrate. The blank sterile filter is composed predominately of O with lesser C.

In order to better classify the size distribution of the particulate material, a single one liter water sample collected on October 6, 2010 was sequentially filtered in a stepwise fashion using cellulose filters which decreased in size. This sample was first filtered using 5.0 μm cellulose filter. The filtered water was then re-filtered using 0.45 μm, 0.22 μm, and 0.05 μm cellulose filters in succession. A small portion of each filter with corresponding particulate material was then mounted on an aluminum SEM stub using a carbon adhesive and Au + Pd coated as noted previously. These samples were then analyzed using energy dispersive spectroscopy (EDS) on the SEM. SEM-EDS analyses, which identify Al, may actually be penetrating both the particulate material and cellulose filter, thus measuring and identifying Al from the underlying aluminum SEM stub.

2.4.2. X-Ray Diffraction. Particulate material filtered in the field using cellulose filters were analyzed using a X'PERT SW X-ray diffractometer. The XRD analysis was a continuous, fast scan with $CuK_{\alpha 1}$ monochromatic x-rays with a wavelength of 1.54056 and a 2θ scan range of 5.015° to 59.975°. The stream particulate

material collected on the 0.45 μm and 0.22 μm cellulosic filters were also used for X-ray diffraction and ICP-OES analyses by halving the filter paper as closely as possible. The particulate material was analyzed on the filter substrate of the 0.45 μm and 0.22 μm filters. Analysis of an unused sterile filter sheet revealed that no crystalline structured material was detected within the blank filter over the 2θ scan range used with the XRD.

2.4.3. Inductively Coupled Plasma – Optical Emission Spectroscopy

Inductively coupled plasma – optical emission spectrometer (ICP – OES) analysis was employed to determine the major constituents of the particulate material collected by filtration from Maramec Spring. For ICP – OES analysis, the solid particulate material filtered *ex situ*, but on site, using the cellulosic filters and vacuum filtration techniques at sample location 1 were digested using undiluted, high purity HNO_3.

ICP-OES analyses were also conducted on the particulate material to determine its chemical composition. The remaining halves of the 0.45 μm and 0.22 μm filters used for TSS and XRD, respectively, were each placed in an ultrasonic cleaner for 30 minutes in 15 mL of a 3% ultra-pure HNO_3 acid solution to remove the particulate material from the filter paper. The filter papers were then re-dried and re-weighed on a four decimal precision balance to determine the amount of material liberated from each filter. Approximately 3 mg of particulate material was liberated from each filter. This particulate material was then further digested using undiluted, ultra-pure HNO_3 to a solution pH of 2 or less and analyzed on the ICP-OES. ICP-OES measured accuracies and calculated precisions for all the elements analyzed are giving in Table 2.3. The precisions are the standard deviations of known standards which were measured periodically throughout analysis. The calculated accuracy of the ICP-OES for the 1ppm quality control standards for Si, Fe, Ca, Mg, K, Na, Mn, and Al are: 1%, 1%, 1%, 7%, 5%, 4%, 1%, and 5%, respectively. The calculated accuracy of the ICP-OES for the 10 ppm quality control standards for Si, Fe, Ca, Mg, K, Na, Mn, and Al are: 1%, 1%, 1%, 6%, 5%, 3%, 1%, and 5%, respectively.

Table 2.3. ICP-OES quality control standards measured values, mean values, and standard deviations for concentrations of 1 and 10 ppm.

	Measured Concentration (ppm)							
Quality Control Standards	**Si**	**Fe**	**Ca**	**Mg**	**K**	**Na**	**Mn**	**Al**
1 ppm	1.00	1.00	1.01	1.07	1.06	1.04	1.02	1.06
1 ppm	0.99	0.99	0.99	1.06	1.03	1.03	1.00	1.04
1 ppm	1.00	1.00	1.00	1.06	1.05	1.04	1.01	1.05
MEAN	0.99	1.00	1.00	1.06	1.05	1.04	1.01	1.05
Standard Deviation	0.01	0.01	0.01	0.01	0.02	0.01	0.01	0.01
10 ppm	9.99	10.20	9.94	10.60	10.50	10.30	10.00	10.40
10 ppm	9.96	9.91	9.98	10.40	10.40	10.20	9.87	10.50
10 ppm	10.00	10.10	9.78	10.60	10.40	10.40	10.10	10.50
MEAN	9.98	10.07	9.90	10.53	10.43	10.30	9.99	10.47
Standard Deviation	0.02	0.15	0.11	0.12	0.06	0.10	0.12	0.06

3. RESULTS

3.1. SOLUTION ANALYSIS

A noticeable increase in pH is observed moving downstream away from the point of upwelling (Figure 3.1, Table A1). The range of data from 12 different sampling dates for pH measurements for sampling locations 1 through 8 are: 6.87 - 7.39, 6.87 - 7.30, 6.77 – 7.39, 7.04 – 7.51, 6.99 – 7.46, 7.22 – 7.59, 7.28 – 7.63, 7.33 – 7.50, respectively. Eh values are observed to decrease slightly downstream with only minor variability, and inversely correlate with measured pH values (Figure 3.2, Table A2).

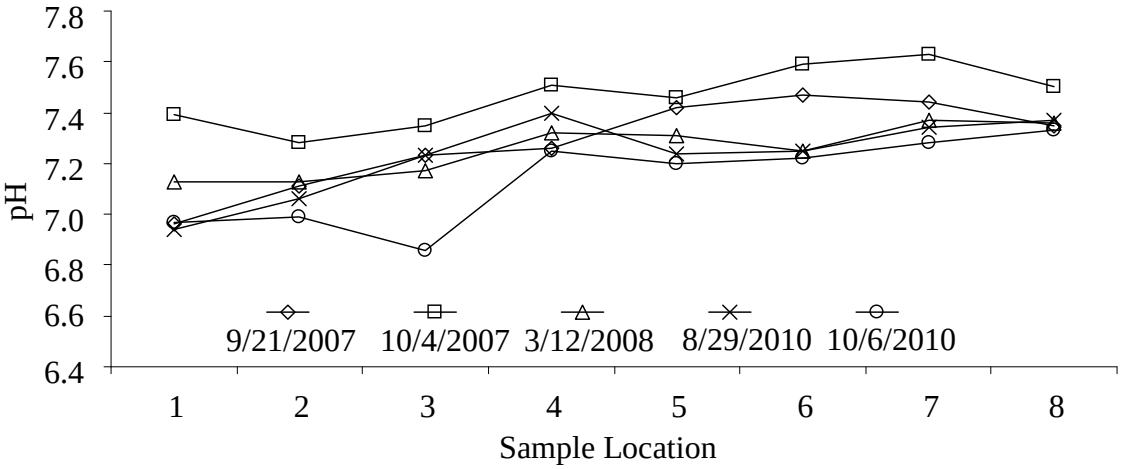

Figure 3.1. Measured pH values of the Maramec Spring's stream waters from the five most recent sample trips. Overall, pH values tend to increase in the downstream direction.

As with the pH measurements, the water temperature of the spring increased slightly downstream. The mean water temperatures for stations 1, 2, 3, 4, 5, 6, 7, and 8 are: 13.8 ± 0.5, 13.7 ± 0.6, 13.7 ± 0.5, 13.9 ± 0.7, 14.2 ± 0.8, 14.1 ± 1.4, 14.2 ± 1.0, 14.3 ± 1.0 ^{o}C, respectively (Figure 3.3, Table A3). The high standard deviations reported for

stations 6, 7, and 8 are due to the lack of data. These stations were only measured on the last three sample trips, and therefore may reflect a statistical variation more than seasonal anomalies. Lowest temperatures were measured during the early spring months whereas the highest recorded temperatures were measured in the late summer.

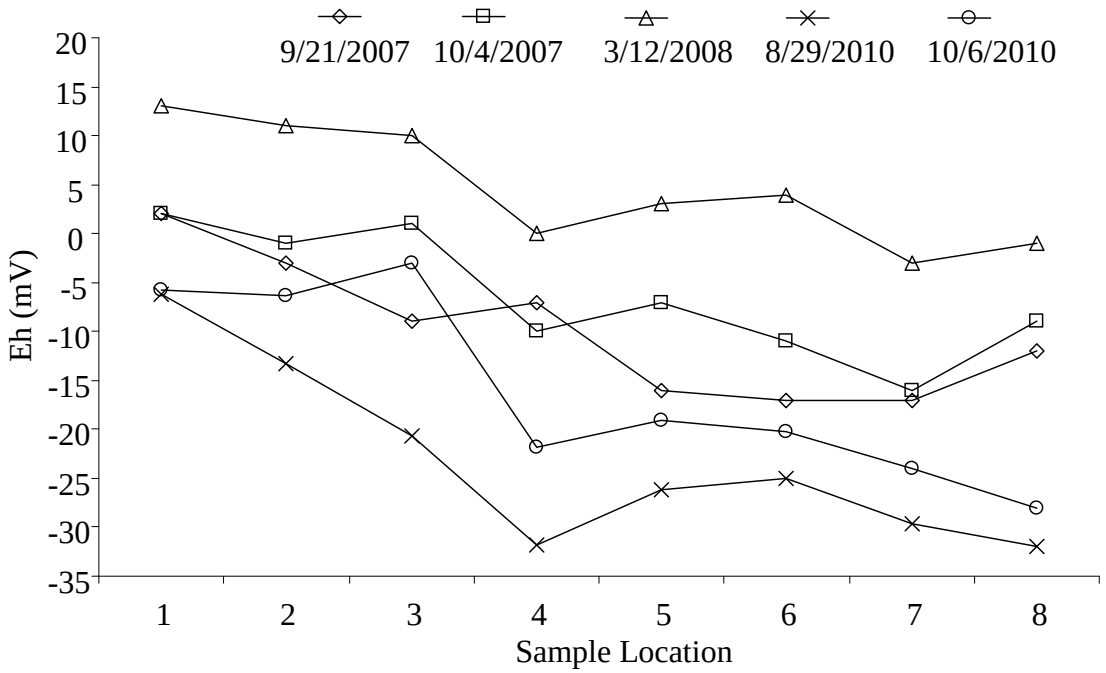

Figure 3.2. Measured Eh values of Maramec Spring's stream waters from the last five sample trips. Eh values are inversely correlated to measured pH values, decreasing in the downstream direction.

Unlike pH, Eh, and temperature, conductivity was relatively consistent throughout the sampling reach of the stream for each individual date sampled. These conductivity measurements tended to be higher on days following local rain events with an overall range for all dates falling between 180.6 and 321.0 μSiemens/cm (Table A4). The amount of TSS and TDS in the spring water were 1.93×10^{-6} g/ml and 2.05×10^{-4} g/ml, respectively.

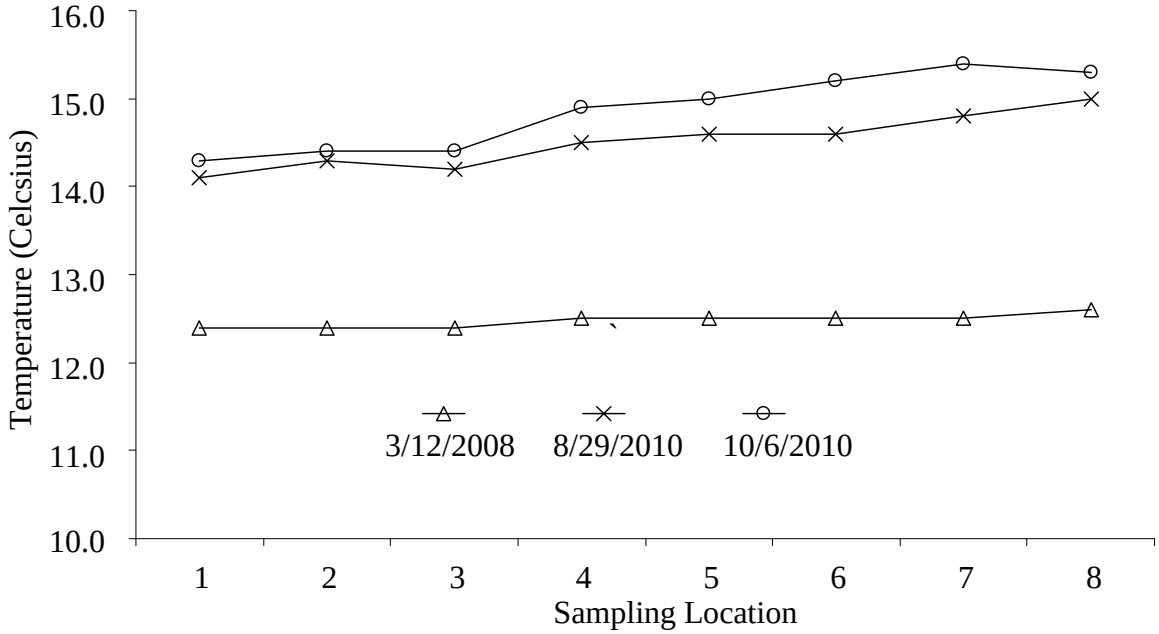

Figure 3.3. Maramec Spring's measured water temperature on the last three sampling trips. Temperature increases in the downstream direction, away from the point of upwelling.

Turbidity of the Maramec Spring waters was measured successfully only on the March 12, 2008 sampling date. Measured turbidities, in NTU's, for stations 1, 2, 3, 4, 5, 6, 7, and 8 were: 7.53 ± 0.04, 7.54 ± 0.04, 7.67 ± 0.04, 7.53 ± 0.04, 7.74 ± 0.04, 8.48 ± 0.04, 8.24 ± 0.04, and 7.78 ± 0.04 (Table A5).

CO_2 flux was measured on one occasion at three sampling locations a few days following a heavy rain. Flux values, in μmoles CO_2/m^2sec, for sampling locations 1, 3, and 5 are: 17.5 ± 3.3, 8.5 ± 3.9, and 2.6 ± 6.1, respectively (Figure 3.4, Table A6).

Total, calcium, and magnesium hardness, as well as alkalinity (buffering capacity) measurements were only preformed on the last two trips (Table A7). These measurements, as with the conductivity measurements, remained relatively constant throughout the spring system on each of the sampling dates. On August 29, 2010, the total, calcium, and magnesium hardness values, as well as alkalinity mean values for stations 1, 2, 3, and 4 are 162 ppm, 90 ppm, 72 ppm, and 162 ppm, respectively.

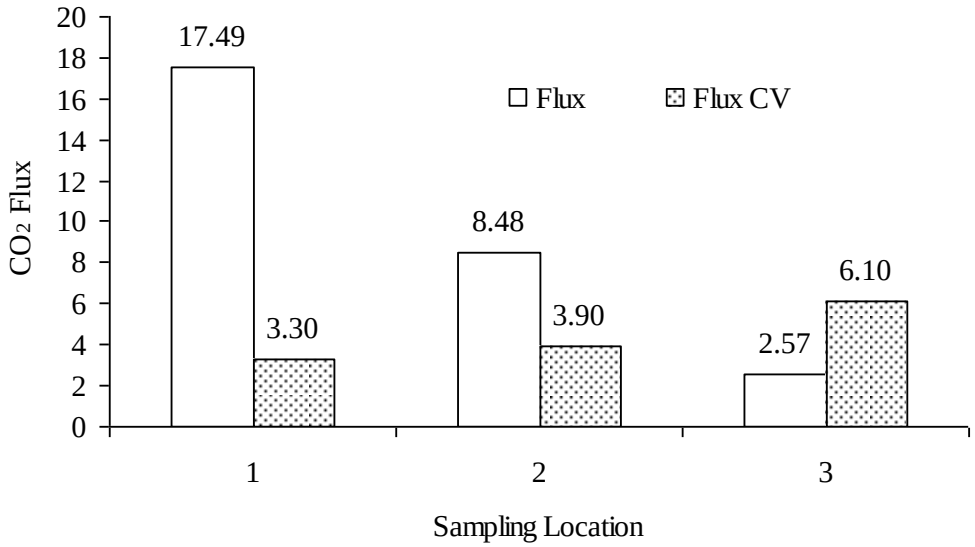

Figure 3.4. Measured CO_2 flux at Maramec Spring. These measurements were collected three days after a heavy precipitation event. Spring turbidity, as well as flow rate, showed a visual increase. The relatively high coefficient of variation (CV) noted at site 5 is believed to be the result of photosynthetic activities of aquatic algae at this location. Measurements are in moles of CO_2/meter^2*second.

ICP-OES analysis of the spring's water was performed on unfiltered and filtered water samples that were filtered on site, but *ex situ*. Filtering the water did not appear to have a significant affect on the chemistry of the water, i.e. the filtered water samples had a similar composition as the unfiltered water samples. Ca was the most abundant cation observed in solution with a mean concentration of 32.96 ± 0.11 ppm (Figure 3.5 and Table 3.1). The second most abundant cation was Mg with a mean concentration of 19.72 ± 0.12 ppm. Si, K, and Na were detected and have mean concentrations of 4.24 ± 0.02 ppm, 1.71 ± 0.01 ppm, and 1.41 ± 0.01 ppm, respectively. Al, Fe, and Mn were below instrument detection limits (Figure 3.6). The sample labeled "5.0 SPIKE" is a water sample collected from the spring with a 6 ppm laboratory standard added.

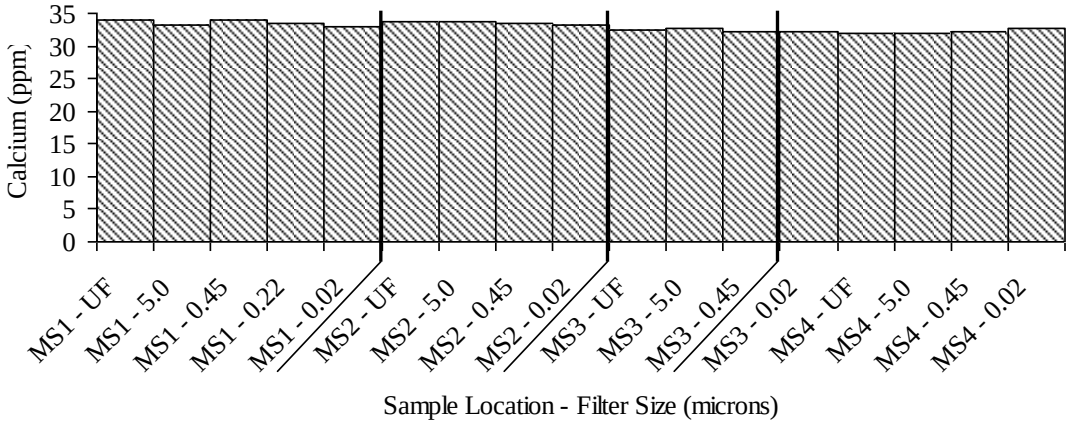

Figure 3.5. Measured calcium concentrations by ICP-OES of unfiltered and filtered water samples collected from sampling locations 1, 2, 3, and 4 on 8/29/2010. Note that there is only minor variation in measured [Ca^{+2}] in the downstream direction. Filtering does not appear to have any effect on the [Ca^{+2}].

Table 3.1. ICP-OES results for unfiltered and filtered water samples and digested particulate material collected on 8/29/2010. Note that there is a noticeable difference between the chemistry of the water samples and digested particulate material. Cations with a negative sign indicates that the sample was below instrument detection limit.

Sample		Concentration (ppm)							
Sample Location	**Filter Size (µm)**	**Si**	**Fe**	**Ca**	**Mg**	**K**	**Na**	**Mn**	**Al**
1	**Unfiltered**	4.30	-0.07	34.00	19.90	1.51	1.38	0.00	-0.04
1	**5.00**	4.26	-0.08	33.30	19.50	1.75	1.44	0.00	-0.04
1	**0.45**	4.29	-0.09	34.10	19.90	1.74	1.45	0.00	-0.05
1	**0.45 DUPLICATE**	4.22	-0.08	32.60	19.60	1.68	1.39	0.00	-0.05
1	**0.22**	4.31	-0.08	33.40	19.90	1.87	1.49	0.00	-0.05
1	**0.02**	4.25	-0.09	33.00	20.00	1.53	1.38	0.00	-0.03
2	**Unfiltered**	4.25	-0.07	33.70	19.70	1.63	1.40	0.00	-0.04
2	**5.00**	4.23	-0.08	33.80	19.90	1.64	1.40	0.00	-0.05
2	**0.45**	4.24	-0.09	33.50	19.90	1.63	1.39	0.00	-0.05
2	**0.02**	4.23	-0.08	33.20	19.90	1.64	1.38	0.00	-0.03
3	**Unfiltered**	4.25	-0.08	32.50	19.30	2.16	1.46	0.00	-0.04
3	**5.00**	4.29	-0.08	32.60	19.90	1.91	1.44	0.00	-0.05
3	**5.00 SPIKED**	10.20	6.30	37.30	25.00	8.22	7.92	6.30	6.64
3	**0.45**	4.19	-0.09	32.10	19.50	1.89	1.43	0.00	-0.05
3	**0.02**	4.22	-0.09	32.30	19.70	1.70	1.40	0.00	-0.03
4	**Unfiltered**	4.19	-0.07	31.90	19.50	1.68	1.36	0.00	-0.04
4	**5.00**	4.17	-0.08	31.90	19.40	1.58	1.35	0.00	-0.05
4	**0.45**	4.15	-0.08	32.30	19.50	1.58	1.35	0.00	-0.05
4	**0.02**	4.20	-0.08	32.70	19.80	1.65	1.39	0.00	0.00
1	**0.45 PARTICULATE**	2.06	0.81	2.69	0.46	1.07	0.39	0.02	1.34
1	**0.22 PARTICULATE**	7.16	2.07	1.27	0.78	1.41	0.65	0.04	3.43

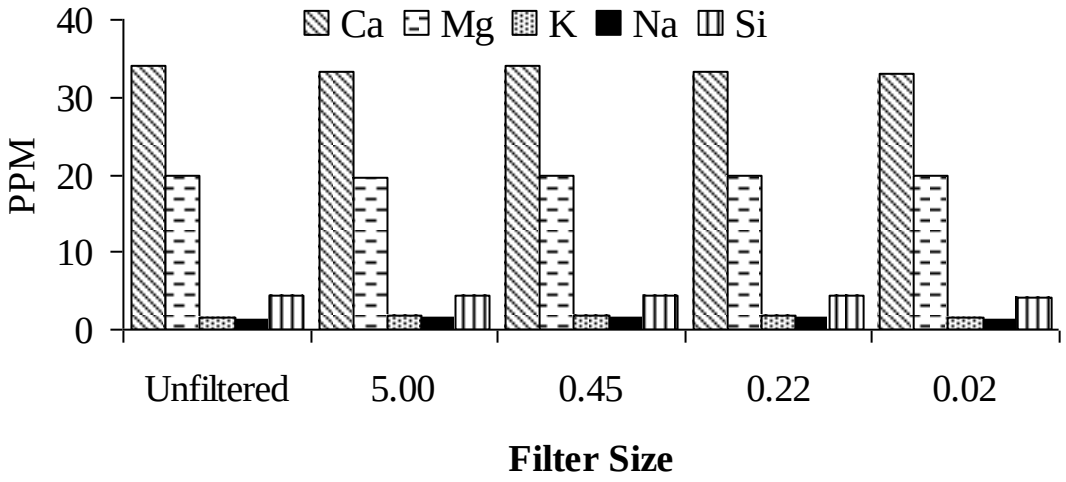

Figure 3.6. ICP-OES of unfiltered and filtered spring water from sampling location 1 collected 8/29/2010. Note that filtering does not appear to have an effect on the water chemistry.

3.2. CENTRIFUGED PARTICULATE ANALYSIS

The suspended particulate material collected from Maramec Spring has been identified as a carbonate mineral with the aid of a 5% HCl solution. This test consisted of centrifuging unfiltered spring water and conducting a "fizz test" on the collected particulate material. Since the precipitate material fizzed readily when put into contact with the weak acid it was assumed to be a carbonate mineral. A Nikon binocular scope with magnification capacity up to 126-X magnification was used at the start of the project to image the crystals, but due to the extremely fine size of the particulate material no sound conclusions could be drawn with respect to the form and habits of the grains. The particulate phase collected from centrifuging spring water was also analyzed on the SEM. The first samples analyzed using the SEM were the samples that were made using the evaporative material on the aluminum stubs and glass slides. The particulate phase has a rhombohedral form and crystal sizes of approximately 10 μm (Figure 3.7). Some organic debris, described as filaments, and occasional diatoms are observed on the SEM. EDS results from the SEM indicate that the particulate phase collected by centrifuging the spring water is predominately composed of calcium (84 atomic %) and magnesium (4

atomic %) (Figure 3.8). The SEM-EDS data is not referenced to a standards thus giving semi-quantitative values.

3.3. VACUUM FILTERED PARTICULATE ANALYSIS

The particulate materials collected on the different sized cellulose filters have visible differences when examined with the naked eye as discussed below (Figure 3.9). An unknown yellow particulate material is observed to be present on the 5.0 μm and 0.45 μm filter fractions and is present in much greater abundance on the 0.45 μm filter when compared to the 5.0 μm. This yellow particulate material is not observed on the 0.22 μm or 0.05 μm filters. The yellow phase does not appear to be texturally different from the material collected on the 0.22 μm or 0.05 μm filters in SEM analyses, but is observed to be compositionally different.

The particulate material collected by sequential filtering using 5 μm, 0.45 μm, 0.22 μm, and 0.05 μm Millipore cellulose filters were also examined in the SEM. Unlike the isolated particles collected after centrifugation (Figure 3.7), a large quantity of particulate material was collected on the filters. This particulate material varied greatly in both quantity and features between filter sizes. The particulate material collected on the 5 μm filter included elongated organic matter, elongated tubular structures, and a subhedral rectangular mineral phase (Figure 3.10). The 0.45 and 0.22 μm filters collected the most material. There is a bimodal size distribution of the particulate material collected upon the filters (Figure 3.11). There is a much finer particulate material that fills the filter's pores. On top of this finer grained particulate material are larger particulates displaying very diverse morphologies. These larger particles are observed to be rectangular to semi-rhombohedral with sharp crystal faces, spherical, elongate tubular, and anhedral in shape (Figure 3.10). The 0.05 μm filter collected the least amount of material. The phases collected on this filter have a rectangular outline and are observed to cluster together (Figure 3.12).

Energy dispersive spectroscopy (EDS) analysis was conducted on the particulate phases during SEM analysis. For the euhedral rectangular phase collected on the 0.45

μm filter EDS spectra display sharp peaks for Si, Al, and S. A very small diffuse peak was observed for iron.

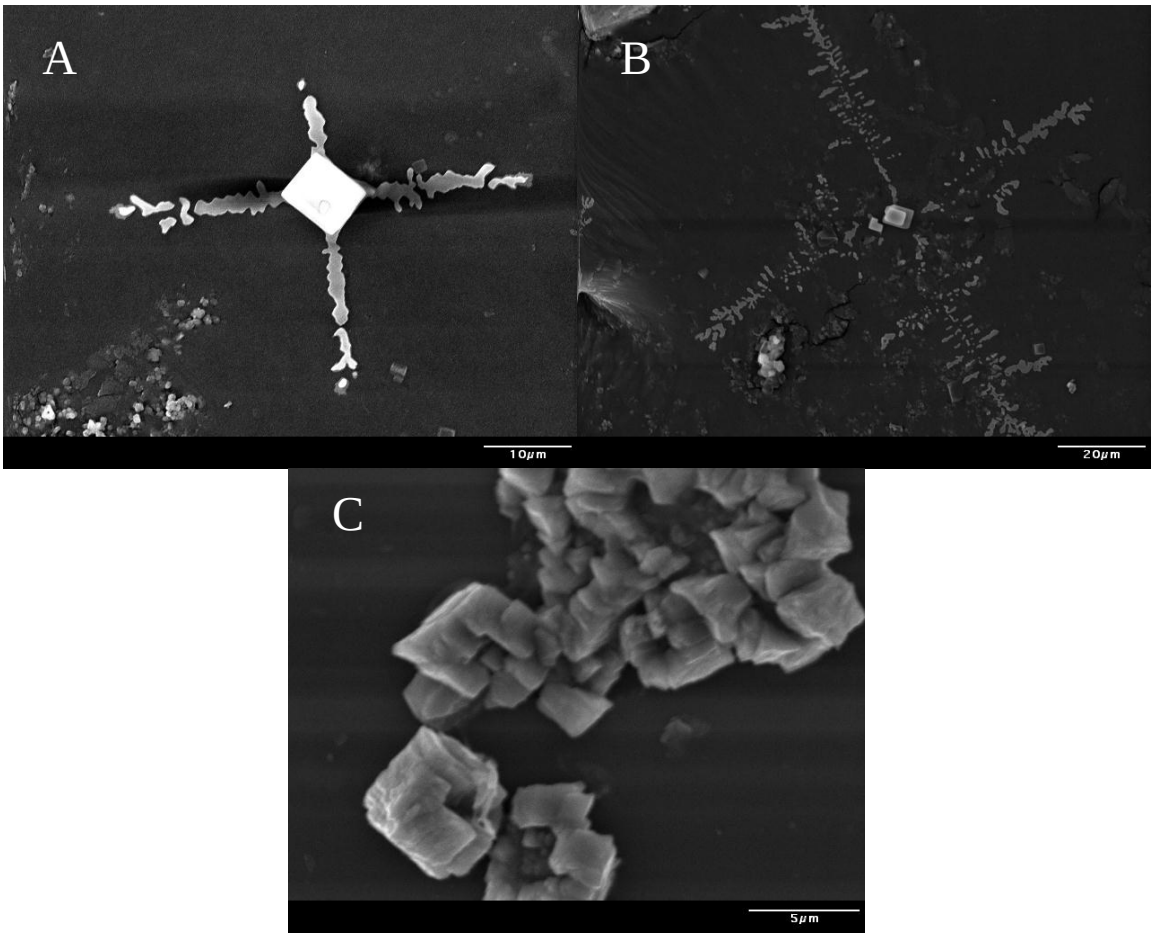

Figure 3.7. Rhombohedral carbonate material collected *via* centrifuging Maramec Spring's water (9/21/2007). (A) A rhombohedral crystals acting as a nucleation point for further calcite growth. The dendritic arms are not a primary feature, but the result of sample preparation including the drying of the sample plus fluid. (B) Larger dendritic structure with a rhombohedral carbonate crystal as a nucleus. (C) A cluster of rhombohedral carbonate crystals.

The rhombohedral phase observed on the 0.22 μm filter displayed sharp peaks for S and to a much lesser extent Si (Figure 3.13.A). The finer grained material (0.5 μm to 1

μm) which fills the pores of the 0.45 and 0.22 μm filters display sharp peaks for Si, Al, O, C, and S (Figure 3.13.B). The rectangular particulate material collected on the 0.05 μm filter displayed a sharp sulfur peak. EDS analysis of a blank filter produced Si, Al, and C peaks. It is important to note that when analyzing small particles using EDS that the resultant x-ray counts may not be generated solely from the particulate material of interest, but also from the surrounding or underlying material.

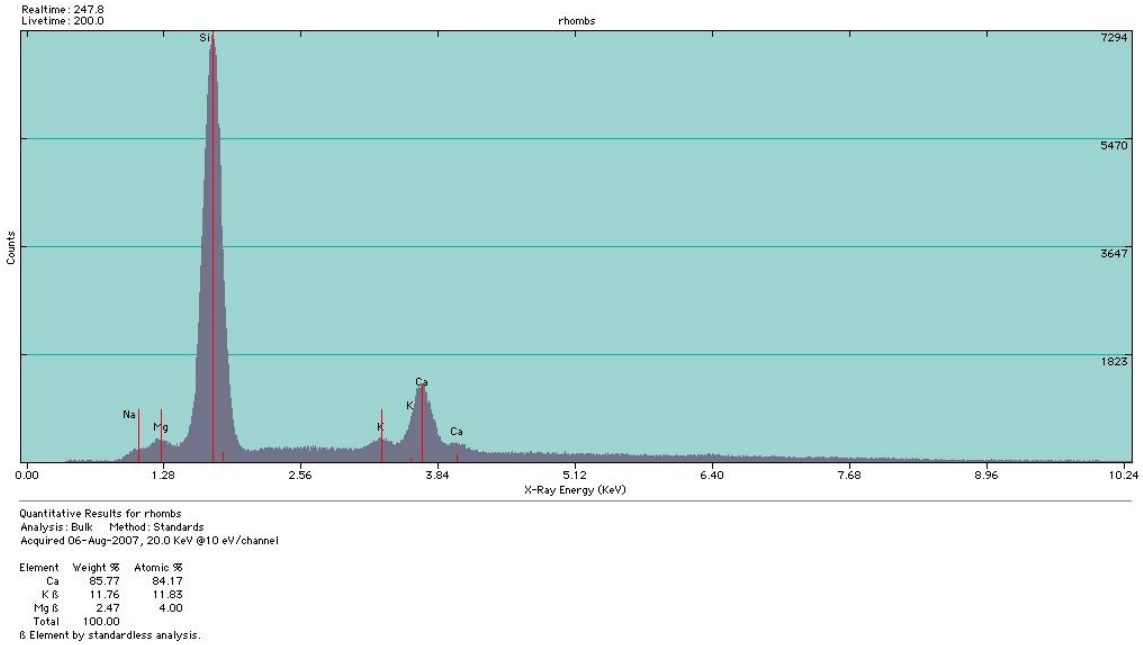

Figure 3.8. EDS spectra of the rhombohedral crystal in Figure 3.7.A. Peaks occur for Si, Ca, Mg, K, and Na. The Si is from the glass slide substrate on which the particulate material was collected on. The K and Na appear to be the result of contamination during sample preparation.

X-ray diffraction (XRD) was conducted on the 0.22 μm cellulose filter plus particulate material. Peaks were observed at 2θ angles of approximately 6.3°, 8.8°, 12.3°, 20.8°, 24.8°, and 26.6° (Figure 3.14). The most prominent peak is at 26.6°. A blank 0.22 μm filter was analyzed by the XRD and did not display any peaks. Thus, all peaks

observed on the filter plus particulate spectrum are interpreted as being valid measurements. The observed peaks appear to be for quartz (20.8° and 26.6°), chlorite or smectite (6.3°, 12.3°, and 24.8°), and illite (8.8°).

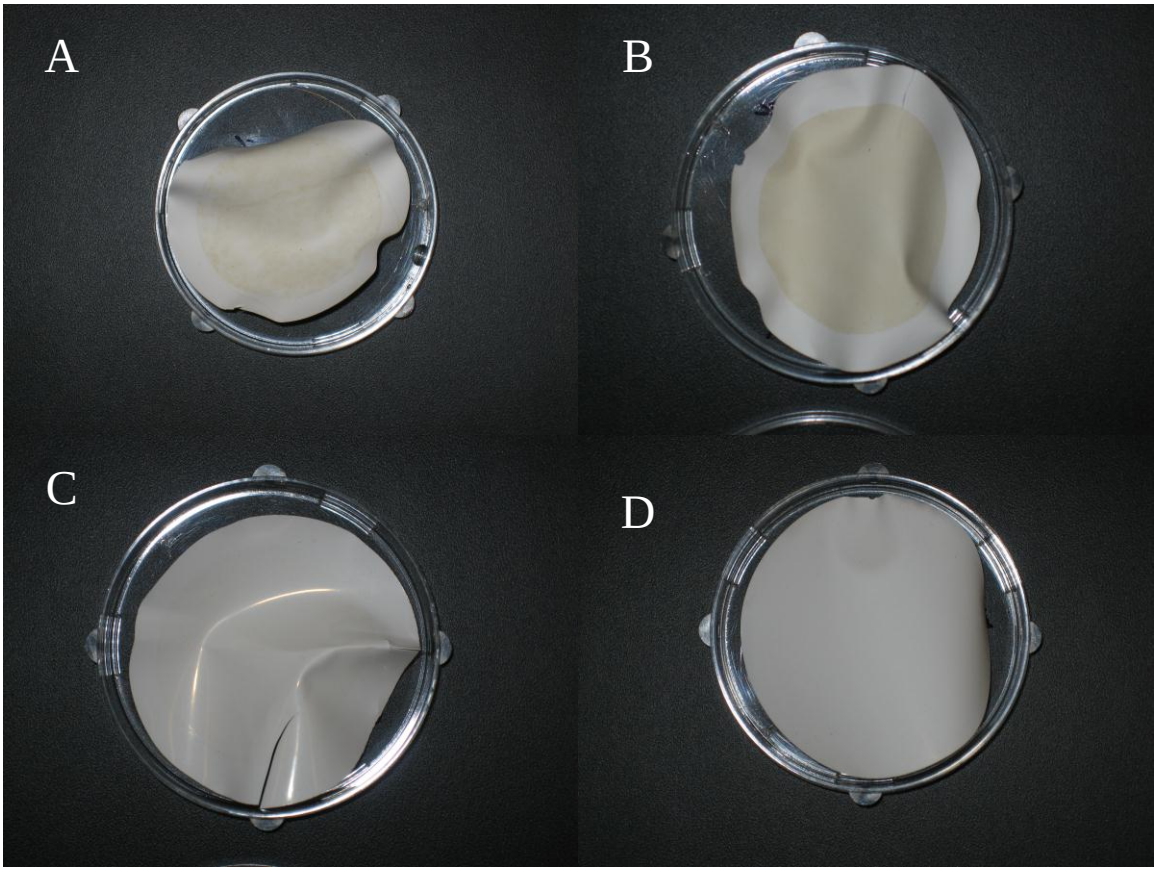

Figure 3.9. Particulate material collected on the (A) 5.0 μm, (B), 0.45 μm, (C) 0.22 μm, and (D) 0.05 μm cellulose filters from sampling location 1 on 10/6/2010. A yellow particulate phase was collected on the 5.0 μm, and 0.45 μm filters (A and B), but is not observed on the 0.22 μm or 0.05 μm (C and D) filters. The diameter of the plastic container is 47 mm.

The ICP-OES analysis of the acid digested particulate material reveals a composition much different than that of the spring waters. Si, Al, Fe, Ca, Mg, Na, and K are all detected (Figure 3.15; Table 3.1). The 0.45 μm particulate material

(predominately yellow) is compositionally different than the 0.22 μm (predominately white) particulate material. Si, Al, and Fe are the major components of the 0.45 μm particulate material, but Ca, Si, Al, Fe, and K are the major components of the 0.22 μm particulate material.

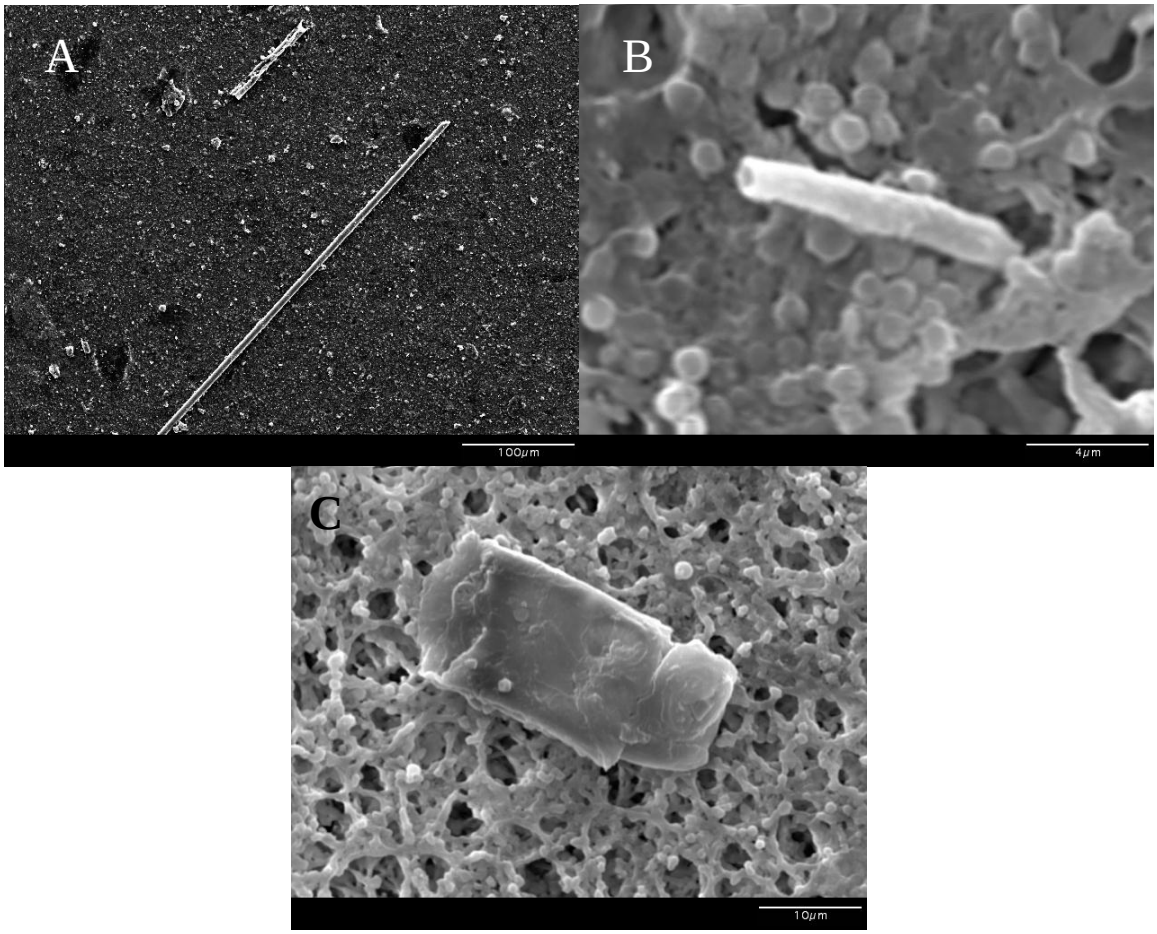

Figure 3.10. Material observed on the 5.0 μm cellulose filter collected on 8/29/2010. Material collected on the filter included (A) filaments, (B) elongate tubular structure, and (C) subhedral blocky particulate material.

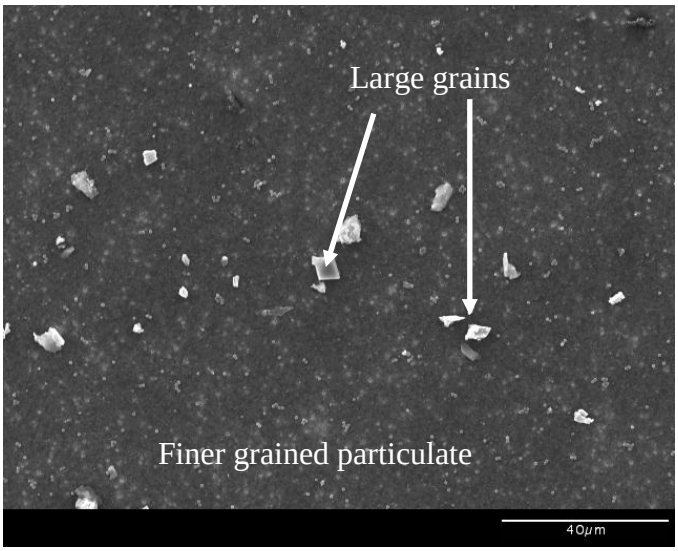

Figure 3.11. Bi-modal size distribution of particulate material collected on the 0.22 μm cellulose filter. The larger particulate grains have anhedral to euhedral forms and are observed sitting on top of a finer grained particulate material.

Figure 3.12. Cluster of particulate material collected on the 0.05 μm cellulose filter.

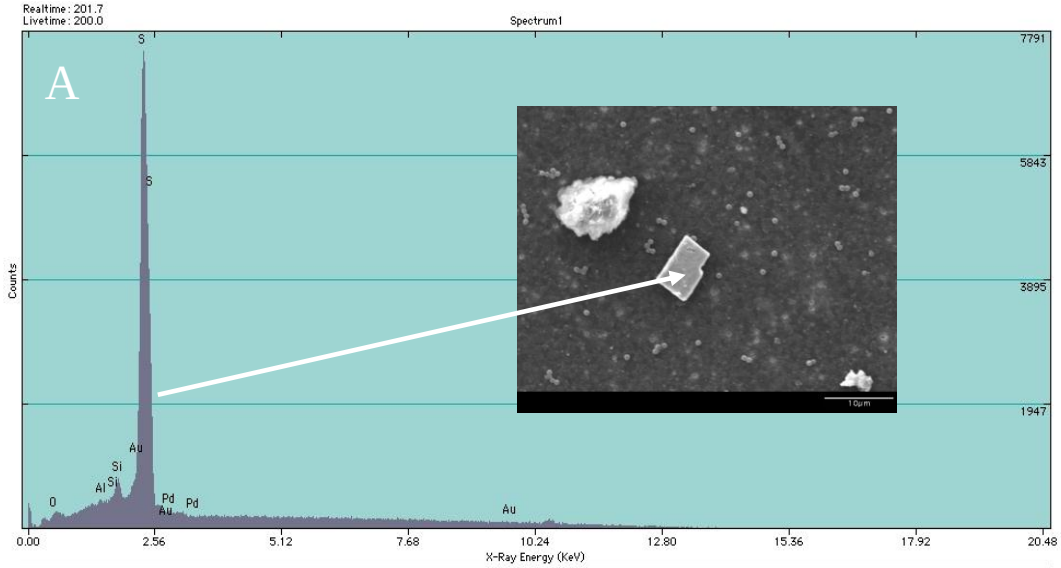

Quantitative Results for Spectrum1
Analysis: Bulk Method: Standardless
Acquired 12-Oct-2010, 15.0 KeV @10 eV/channel

Element	Weight %	Atomic %
Oxygen	3.27	6.89
Aluminum	0.79	0.99
Silicon	3.13	3.77
Sulfur	81.82	86.12
Palladium	2.37	0.75
Gold	8.62	1.48
Total	100.00	

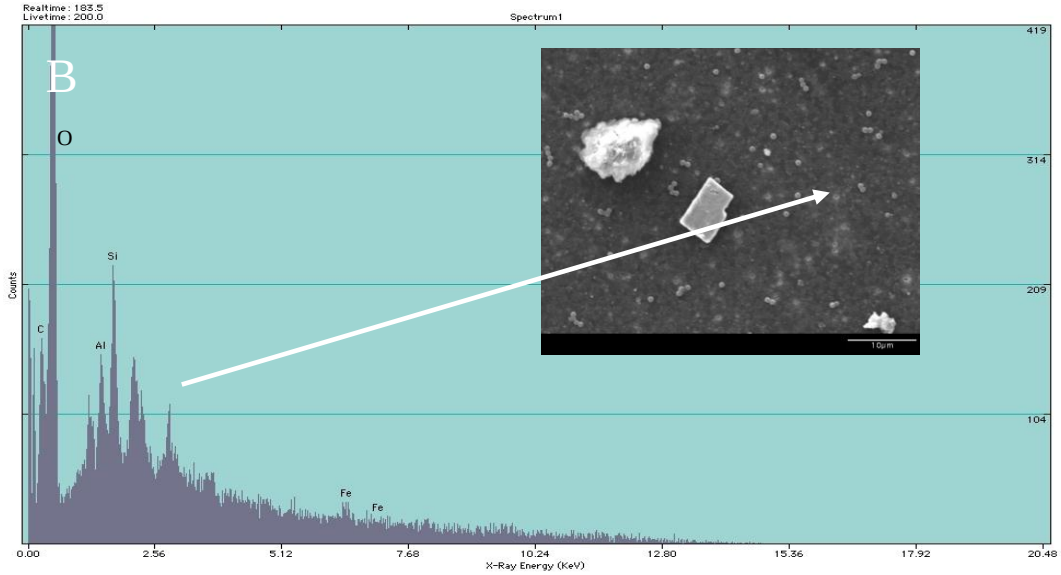

Figure 3.13. Energy Dispersive Spectrum (EDS) for a cubic mineral phase (A) and finer grained particulate material (B) collected on the 0.22 μm cellulose filter. Note the difference in composition of the two materials.

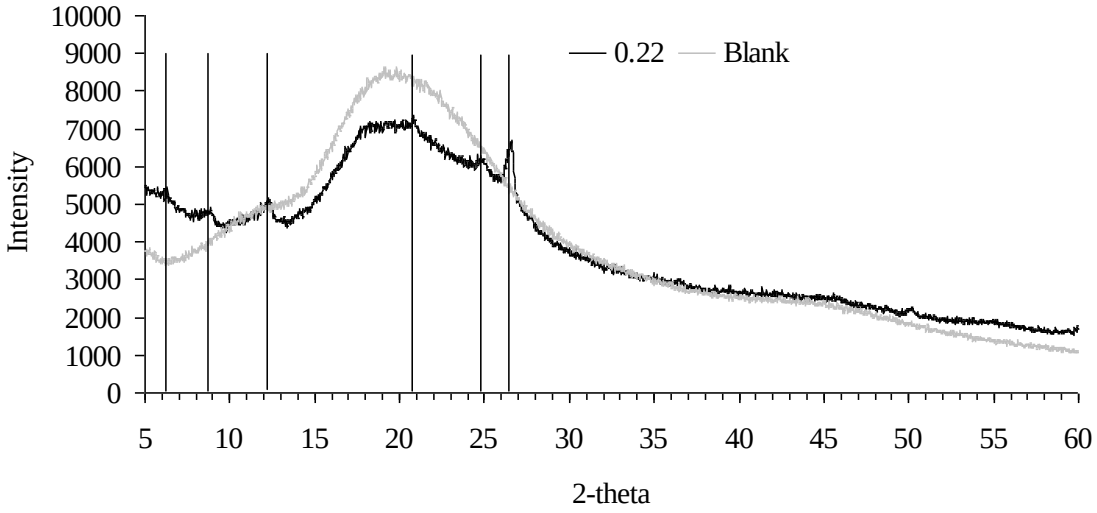

Figure 3.14. X-ray diffraction spectra for particulate material collected on a 0.22 μm from 8/29/2010. Peaks are observed at 2θ angles of 6.3°, 8.8°, 12.3°, 20.8°, 24.8°, and 26.6°. "Blank" refers to the XRD spetra collected on an unused 0.22 μm filter.

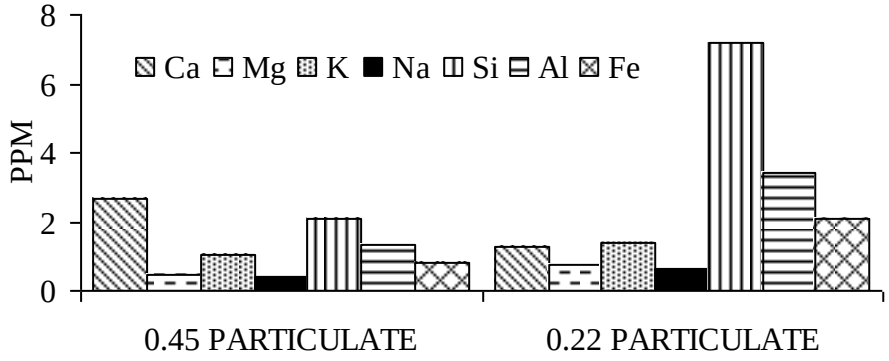

Figure 3.15. ICP-OES analysis of the digested particulate material collected on the 0.45 μm and 0.22 μm cellulose filters at sampling location 1 on 10/6/2010. Note the varying composition between the two filter sizes.

4. DISCUSSION

The chemistry of the Maramec Spring system greatly favors the precipitation of calcium carbonate. This hypothesis is supported by the rhombohedral material collected by centrifuging Maramec Spring's water. The chemical reactions necessary for the precipitation of $CaCO_3$ are (Stumm and Morgan, 1996; Langmuir, 1997; Anderson, 2002; Drever, 2002):

$$CO_2(g) \leftrightarrow CO_2(aq) \quad (1)$$

$$H_2O + CO_2(aq) \leftrightarrow H_2CO_3(aq) \quad (2)$$

$$H_2CO_3(aq) \leftrightarrow H^+ + HCO_3^- \quad (3)$$

$$CaCO_3 + H^+ \leftrightarrow Ca^{+2} + HCO_3^- \quad (4)$$

The Maramec Spring waters have been calculated to be slightly undersaturated to saturated in Ca, with respect to all calcium carbonate polymorphs, but close to equilibrium. Using Visual MINTEC freeware saturation indices (i.e. $(\alpha Ca^* \alpha CO_3^{-2})/K_{sp}$ of Calcite) were calculated at a fixed pH and temperature of 6.97 and 14.3°C, respectively, using the following parameters: $[Ca^{+2}]$ of 34 mg/l, $[Mg^{+2}]$ of 19.9 mg/l, and $[CO_3^{-2}]$ of 144 mg/l. MINTEC calculated the spring waters to have a saturation index for calcium of -0.994 mg/l with respect to calcite. These values are measured values of the unfiltered spring waters collected from sampling location 1 on August 29, 2010. The saturation index of the spring water likely varies from day to day and is influenced by various factors, especially temperature and local precipitation events. The vaules for Ca and Mg were determined by ICP-OES analsis while alkalinity was determined by colorametric titration using HACH field kits. Calcium carbonate precipitation can be achieved *via* Ca^{+2} and CO_3^- ion binding resulting in amorphous calcium carbonate clusters which then transform into crystalline calcite (Gebaur et al., 2008), or by changing the spring water chemistry (i.e. CO_2 degassing).

Multiple mechanisms for calcium carbonate precipitation have been proposed. Wilson (1975) described eight mechanisms that encourage the precipitation of $CaCO_3$. They are: an increase in temperature, increased evaporation, influx of Ca supersaturated

water to $CaCO_3$ nucleation sites, upwelling from higher pressure to lower pressure, mixing of waters with high [CO_3^{-2}] and low [Ca^{+2}] with sea water, organic processes in body fluids, bacterial decay producing ammonia, rising pH with increased carbonate concentration, and CO_2 removal via photosynthetic processes. Measurements collected *in situ* at Maramec Springs (i.e. pH, CO_2 flux, and temperature) support calcium carbonate precipitation through a mechanism involving the degassing of CO_2. Theoretically, as the spring waters upwell from depth within the conduit there will be a decrease in pressure. This decrease in pressure would effectively reduce the amount of CO_2 dissolved in solution for the spring waters forcing its escape from the water and into the atmosphere. The observed temperature increase along the Maramec Spring branch, although minor, will further aid in the degassing of CO_2. This hypothesis is supported by *in situ* CO_2 flux measurements which show that CO_2 is being degassed at the point of upwelling at Maramec Spring (Figure 3.4). Using the chemical reactions outlined above, the process of degassing CO_2 from solution would cause reaction (1) to be driven to the left. In order for the system to maintain equilibrium, reactions (2), (3), and (4) must also proceed left. If these reactions all proceed at the same rate, then there should be no measured change in pH, and one mole of CO_2 (g) should be produced for every mole of $CaCO_3$(s) precipitated. However, if equation (3) is forced to the left at a faster rate than equation (4), then an increase in solution pH should be observed and the $CaCO_3$(s) precipitation will still be linked to CO_2(g), but not in a quantitative sense. Calcium carbonate (calcite) is precipitated *via* the mechanism depicted in equation (4) as it moves to the left provided the activity of Ca is at or above the saturation level. When the Maramec Spring waters are saturated to supersaturated in calcium, with respect to calcite, the degassing of CO_2 from solution, reaction (1), is believed to be the rate limiting step for calcium carbonate precipitation (Lebron and Suarez, 1996, Dreybrodt et al., 1997; Zhang and Grattoni, 1998).

Unlike the pH increase measured along the Maramec Spring stream reach, many experimental laboratory studies have observed a pH decrease upon the onset of calcium carbonate precipitation (Reddy and Nancollas, 1971; Lakshtanov and Stipp, 2010). This disagreement arises because reactions (3) and (4), moving right to left, both may influence solution pH of the system. In reaction (4), moving right to left, hydrogen ions

are produced, thus lowering solution pH. Conversely, in reaction (3) hydrogen ions are consumed and solution pH increases. Calcium carbonate precipitation from supersaturated solutions will also cause reaction (4) to move to the left. In a scenario of supersaturated solution, reaction (4) is the rate limiting step in calcium carbonate precipitation. In an attempt to maintain chemical equilibrium reactions (1), (2), and (3) are forced to move to the left in response to reaction (4). If this process results in the number of hydrogen ions produced in reaction (4) to outpace the rate hydrogen ions that are consumed in reaction (3), then a pH decrease should be observed when precipitating calcium carbonate from supersaturated solutions. For example, calcium carbonate crystallization occurs very rapidly at first (i.e. reaction (4) is the rate limiting step), and slows as the solution approaches equilibrium (Kamkha et al., 1989; Dove and Hochella, 1993; Gómez-Morales et al., 1996; Teng et al., 2000; Dickinson et al., 2002; Lakshtanov and Stipp, 2010).

A comparison of all experimental results suggests that calcium carbonate precipitation in Maramec Spring is induced by CO_2 degassing rather than due to $[Ca^{+2}]$ in solution being supersaturated, i.e. reaction (1). Evidence for this conclusion includes CO_2 degassing (Figure 3.4), pH rise in solution (Figure 3.1), and solution $[Ca^{+2}]$ that are near saturation for calcite, but not highly supersaturated. This process causes reactions (1), (2), (3), and (4) to be forced to react to the left in sequence, resulting in an overall pH increase. This pH increase occurs because reaction (4) is dependent upon reaction (3) since reaction (1) is the rate limiting step. Essentially, more hydrogen ions are consumed much quicker during calcium carbonate precipitation in this system than produced. In laboratory experiments which utilize calcium supersaturated solutions to induce precipitation reactions occur in reverse order, i.e. (4), (3), (2), then (1), causing more hydrogen ions to produced much quicker than they are consumed.

Evidence that supports precipitation of carbonate material in the spring rather than transportation of the carbonate particulate material from other locations in the cave includes composition of the centrifuged particulate material (i.e. calcite rather than dolomite), the euhedral crystal shapes (Figure 3.6), and measured pH increase along the Maramec Spring stream reach. The predominately Ca composition of the particulate phase reflects the chemistry of the water, but may also be the result of many other

examples including non-biogenic calcium carbonate or the presence of kinetic inhibitors preventing dolomite formation. The pH increase and water chemistry both favor calcium carbonate precipitation as outlined above. The euhedral crystal shapes further supports a model invoking the precipitation from solution rather than erosion and transportation from the Gasconade Formation since the sharp corners of the crystal are preserved. During transportation these corners would be physically rounded or abraded. Additional support is the absence of defects, i.e. dissolution pits, on the crystal surface. Transported crystals eroded from the host rock would be expected to have evidence of chemical weathering processes. Based upon the evidence stated above, the reaction with 5% HCl of the particulates, and the measured SEM-EDS composition, the precipitate material collected by centrifuging spring water appears to be calcite. Analysis of the particulate material collected *via* centrifuging the spring water supports the hypothesis that the particulate material precipitated within Maramec Spring is calcite whose precipitation is induced by CO_2 degassing.

Samples collected by way of vacuum filtration are mineralogically and geochemically different than the particulate material collected through centrifuging spring waters using cellulose filters. The particulate material collected by sequential filtering of one liter of spring water is composed of primarily of Si and Al. This suggests that the particulate material causing the milky blue color at Maramec Spring may simply be suspended clays or clays mixed with other particles. The presence of calcite, quartz, illite, chlorite, smectite, or kaolinite were confirmed by SEM-EDS, XRD, and ICP-OES and are summarized in Table 4.1. Results of EDS analyses of large particulate grains are different from those of the finer particulate grains which comprise the bulk of the >5.0 μm, 5.0 - 0.45 μm, and 0.45 - 0.22 μm filter fraction samples. The large particulate grains have a distinct S peak which is not observed in the EDS spectra for the finer particulate grains. Both the large particulate grains and finer particulate grains display sharp peaks for Si and Al with a broad peak for Fe (Figure 3.13). The cubic material clusters collected on the 0.05 μm sample also display a sharp EDS spectra peak for peak for S.

XRD analysis confirmed the presence of clays by displayed peaks at 2θ angles of 6.3°, 8.8°, 12.3°, 20.8°, 24.8°, and 26.6° (Figure 3.14). The other peaks correspond to the

Table 4.1. Summary of all analyses conducted on the particulate material collected from Maramec Spring sampling location 1. Cations are listed in order of decreasing concentration or quantity.

	Observations/Results				
Sample	**Color**	**Morphology**	**SEM-EDS**	**ICP-OES**	**XRD**
Centrifuged	White and Yellow	Rhombohedral	Ca, Mg	-	-
5.0 µm Filter	Yellow	Rectangular	Si, Al, S, Fe	-	-
0.45 µm Filter	Yellow	Rectangular	Si, Al, S, Fe	Ca, Si, Al, K, Fe, Mg, Na	-
0.22 µm Filter	White	Rhombohedral	Si, S	Si, Al, Fe, K, Ca, Mg, Na	Quartz, Illite, Smectite or Kaolinite (Chlorite?)
0.22 µm Filter	White	Finer grained	Si, Al, O, C, S	Si, Al, Fe, K, Ca, Mg, Na	Quartz, Illite, Smectite or Kaolinite (Chlorite?)
0.05 µm Filter	White	Rectangular	S	-	-
Blank Filter	-	-	O, C	-	-

clay minerals kaonilinte, chlorite, or smectite (6.3°, 12.3°, and 24.8°), and illite (8.8°). The peaks for chlorite overlap with kaolinite and smectite clays and thus are difficult to distinguish from one another. Additional analyses are needed to confirm this hypothesis. Given the post-depositional geological history of the host rocks the clays are most likely kaolinite and smectite. Kaolinite is mined from paleo-sinkoles around the Rolla area (Keller et al., 1954). The kaolinite clays are the result of weathering the Precambrian basement rocks. These diagenetic clays were deposited in sinkholes. Over time, leaching increased the grade of the clay deposits making them economical in Missouri. The most dominant peaks are observed at a 2θ angle of 20.8° and 26.6° which are indicative of quartz. The height of the quartz peaks at 20.8° and 26.6° suggest that quartz may be the dominant phase present, but SEM-EDS analysis does not support this hypothesis. The quartz may fills the filter's pores and is thus detected using SEM-EDS, but cannot be physically seen on the SEM. Perhaps the intensity of the peaks at angles of 20.8° and 26.6° is reflects how efficient quartz is able to diffract the x-rays in comparison to the clay minerals.

The absence of a distinct calcium carbonate phase from the vacuum filtered samples cannot be easily explained since calcite was collected by centrifuging the spring water. One hypothesis which can be used to explain this absence is that filtering the water samples under vacuum causes pressure sensitive phases (i.e. calcium carbonate) to dissolve. Another hypothesis is that the calcium carbonate material is smaller than 0.05

μm, and was not collected in the finest filter sizes used. This latter hypothesis seems highly unlikely since the calcite which was found in the centrifuged samples was approximately 5 μm across. The calcite crystals may have grown in size after collection through the loss of CO_2 influencing the Ca saturation level with respect to calcite. It is highly plausible that the calcite crystal could increase in size by 1 to 2 μm. A third hypothesis is that the calcium carbonate material is still being precipitated from solution, but just not in as large of quantity as previously assumed. The calcite may be intermixed with the colloidal clays, but below the detection limits of the instrumentation utilized in this study (e.g., XRD). SEM analysis should be able to image sub-micron colloidal material, but EDS may not necessarily be able to accurately identify the materials composition at such substantial magnification. It is important to reiterate that calcite grains have been collected from the spring waters by centrifuging.

5. CONCLUSIONS

To summarize, a positive identification of the colloidal material present within Maramec Spring that gives the springs water its milky blue color cannot be confidently made at this time. The 0.45 μm and 0.22 μm filters trapped the largest volume of particulate material after filtration of Maramec Spring waters. A yellow color is observed in the particulate material collected on the 5.0 μm and 0.45 μm cellulose filters. The yellow particulate material collected on the 0.45 μm has a chemical composition of dominantly Si, Al, and Fe. A white particulate material is observed on the 0.22 μm and 0.05 μm filters. The material collected on the 0.22 μm filter particulate has a chemical composition dominantly composed of Ca, Si, Al, and Fe. Given the results of the ICP-OES, SEM-EDS and XRD analyses on the particulate material collected on the 0.22 μm filter it is hypothesized that calcite, quartz, chlorite, kaolinite and/or smectite, and illite are present in the Maramec Spring water. Further analyses are needed to positively identify the mineralogy of the particulate phases observed, determine their relative proportions, and to determine whether they are in a large enough abundance to give the spring waters a milky blue color. The colloidal particulate material collected on the 0.45 μm filter may also be comprised of clay minerals given the XRD and ICP-OES results, but not necessarily be the same as the clay minerals observed on the 0.22 μm filter.

The observed pH increase of the spring water at Maramec Spring is believed to be induced as a result of CO_2 degassing. This degassing process theoretically favors the precipitation of calcium carbonate from solution. Initially, it was hypothesized that the milky blue color resulted from the precipitation of calcium carbonate induced by CO_2 degassing and an increase in temperature. Particulate material collected *via* centrifuging the spring's water supported this hypothesis. The particulate material, identified as calcite, has a rhombohedral morphology, is composed predominately of Ca with minor amounts of Mg, and reacts with weak HCl acid. Additional attempts to isolate the particulate material using a vacuum filtration sampling technique directly at the Maramec Springs site shows that clay minerals of kaolinite, smectite, or chlorite, illite, and colloidal quartz are the dominant particulate phases collected. SEM-EDS, ICP-OES, and XRD all support this hypothesis. XRD analyses show strong peaks for quartz when

analyzing the 0.22 μm filter and particulate material, but SEM-EDS examination of filter's trapped particles did not reveal the presence of any quartz.

The discrepancies observed between the two different sampling techniques (i.e. centrifuging spring water vs. vacuum filtration) show that sampling methods should be evaluated very carefully. Pressure sensitive phases, such as calcium carbonate, may be selectively dissolving during filtration, thus skewing the particulate fractions. Conversely, calcium carbonate may only be a minor fraction of the particulate material present within the spring water. The only phase observed in both the centrifuged spring water and the vacuum filtration analyses is the yellow particulate phase observed on the 5.0 μm and 0.45 μm filters. This phase is speculated to be suspended clay minerals from the Maramec Spring pool floor or eroded from the host rocks within the spring system recharge area. At this time the primary colloidal material present within Maramec Spring is a mixture of calcite, colloidal quartz, and clay particles. It is not known which phase gives the springs their milky blue color, assuming a particulate phase is responsible for the milky blue color. XRD peaks from the 0.22 μm filters were the most intense for quartz, suggesting this may be the dominant phase present. Caution is exercised here with this interpretation as phase abundance is only one of several factors affecting XRD peak heights.

Future studies should include the sampling of sediments within the spring conduit to determine if the hypothesized clay particulate material or another particulate phase is being suspended from the Maramec Spring pool floor. Also, sampling the spring waters at depth within the conduit may also provide better insight as to how the system behaves before rising to the surface, although this would require the aid of divers. A different filtering technique may be employed to confirm that pressure sensitive phases are not being selectively dissolved during sampling, thus producing a skewed representation of the particulate phases present within the spring waters. Filtration under lower pressures may increase filtration time, potentially allowing mineral phase preservation, or possibly even growth as was observed in the centrifuged samples.

Theoretically, the Maramec Spring system could provide some insight on natural systems acting as both CO_2 sources and reservoirs. Following the simplified model outlined at the beginning of the discussion, CO_2 is being dissolved into groundwater in

the recharge portion of the spring system due to the absorption of CO_2 from the atmosphere, soil gases, and the dissolution of the carbonate bedrock that hosts the spring system. This CO_2 is transported though the spring system in solution as H_2CO_3(aq), HCO_3^-, CO_3^{-2}, and CO_2(aq), and in potentially suspended carbonate particulate phases such as calcite. Some of this CO_2 is then released back into atmosphere as a gas at the point of upwelling. This natural system provides valuable insight into how solution chemistry may influence CO_2 precipitation as carbonate phases following a decrease in pressure. Such processes may cause precipitation to occur in areas where potential future CO_2 repositories develop leaks along fractures. Such a process could theoretically cause a leaking system to self-seal by precipitating carbonate minerals along the fracture system. This process also provides an analogue to evaluate carbonate precipitation events occurring in the carbonate platform settings such as the Red Sea or Bahamas.

APPENDIX

Table A1. Maramec Spring measured water pH.

		Sampling Location								
Measurement	**Date**	**1**	**2**	**3**	**4**	**5**	**6**	**7**	**8**	**Maremec River**
pH	6/14/2001	7.13	7.30	7.39	7.48	-	-	-	-	-
	6/13/2002	6.89	7.14	7.10	7.31	-	-	-	-	-
	6/20/2002	7.06	7.10	7.16	7.20	-	-	-	-	-
	6/28/2002	7.15	7.13	7.22	7.38	7.44	-	-	-	-
	6/12/2003	7.05	7.06	6.77	7.14	7.22	-	-	-	-
	6/20/2003	6.87	6.87	6.94	7.04	6.99	-	-	-	-
	6/27/2003	6.95	7.00	7.06	7.14	7.26	-	-	-	-
	7/10/2007	7.07	7.05	7.26	7.34	7.35	-	-	-	-
	9/21/2007	6.96	7.11	7.23	7.26	7.42	7.47	7.44	7.35	
	10/4/2007	7.39	7.28	7.35	7.51	7.46	7.59	7.63	7.50	8.32
	3/12/2008	7.13	7.13	7.17	7.32	7.31	7.25	7.37	7.36	8.08
	8/29/2010	6.94	7.06	7.23	7.40	7.24	7.25	7.34	7.37	-
	10/6/2010	6.97	6.99	6.86	7.25	7.20	7.22	7.28	7.33	-
pH Check	6/14/2001	-	-	-	-	-	-	-	-	-
(7.0 standard)	6/13/2002	-	-	-	-	-	-	-	-	-
	6/20/2002	-	-	-	-	-	-	-	-	-
	6/28/2002	-	-	-	-	-	-	-	-	-
	6/12/2003	-	-	-	-	-	-	-	-	-
	6/20/2003	-	-	-	-	-	-	-	-	-
	6/27/2003	-	-	-	-	-	-	-	-	-
	7/10/2007	-	-	-	-	-	-	-	-	-
	9/21/2007	7.00	6.98	6.96	7.05	7.05	7.05	7.05	7.05	-
	10/4/2007	7.08	7.10	7.11	7.10	7.13	-	7.10	-	-
	3/12/2008	7.04	7.05	7.05	7.05	7.06	7.07	7.06	7.05	7.07
	8/29/2010	6.99	7.04	6.99	7.00	6.99	7.01	7.00	7.00	-
	10/6/2010	7.00	7.01	7.00	7.00	6.96	7.00	7.00	6.97	-

Table A2. Maramec Springs measured Eh values.

		Sampling Location								
Measurement	**Date**	**1**	**2**	**3**	**4**	**5**	**6**	**7**	**8**	**Maremec River**
Eh	6/14/2001	-	-	-	-	-	-	-	-	-
(mV)	6/13/2002	-	-	-	-	-	-	-	-	-
	6/20/2002	-	-	-	-	-	-	-	-	-
	6/28/2002	-	-	-	-	-	-	-	-	-
	6/12/2003	-	-	-	-	-	-	-	-	-
	6/20/2003	-	-	-	-	-	-	-	-	-
	6/27/2003	-	-	-	-	-	-	-	-	-
	7/10/2007	-4.0	3.0	-5.0	-10.0	-13.0	-	-	-	-
	9/21/2007	2	-3.0	-9.0	-7.0	-16.0	-17.0	-17.0	-12.0	-
	10/4/2007	2	-1.0	1.0	-10.0	-7.0	-11.0	-16.0	-9.0	-60.0
	3/12/2008	13	11.0	10.0	0.0	3.0	4.0	-3.0	-1.0	-41.0
	8/29/2010	-6.2	-13.3	-20.6	-31.8	-26.2	-25.0	-29.7	-32.0	-
	10/6/2010	-5.8	-6.4	-3.0	-21.8	-19.1	-20.3	-24.0	-28.1	-

Table A3. Maramec Spring measured water temperature.

		Sampling Location								
Measurement	**Date**	**1**	**2**	**3**	**4**	**5**	**6**	**7**	**8**	**Maremec River**
Temperature	6/14/2001	14.0	13.9	13.9	14.1	-	-	-	-	-
(^{o}C)	6/13/2002	14.2	14.0	14.2	14.3	-	-	-	-	-
	6/20/2002	14.0	14.1	14.0	14.3	-	-	-	-	-
	6/28/2002	14.3	13.7	13.8	14.2	14.4	-	-	-	-
	6/12/2003	13.6	13.3	13.6	13.6	14.4	-	-	-	-
	6/20/2003	13.6	13.4	13.4	13.5	14.0	-	-	-	-
	6/27/2003	13.6	13.5	13.6	13.7	14.1	-	-	-	-
	7/10/2007	13.7	14.1	13.7	14.0	14.7	-	-	-	-
	9/21/2007	-	-	-	-	-	-	-	-	-
	10/4/2007	-	-	-	-	-	-	-	-	-
	3/12/2008	12.4	12.4	12.4	12.5	12.5	12.5	12.5	12.6	9.5
	8/29/2010	14.1	14.3	14.2	14.5	14.6	14.6	14.8	15.0	-
	10/6/2010	14.3	14.4	14.4	14.9	15.0	15.2	15.4	15.3	-

Table A4. Maramec Spring measured water conductivity.

		Sampling Location								
Measurement	**Date**	**1**	**2**	**3**	**4**	**5**	**6**	**7**	**8**	**Maremec River**
Conductivity	6/14/2001	-	-	-	-	-	-	-	-	-
(μSiemens/cm)	6/13/2002	-	-	-	-	-	-	-	-	-
	6/20/2002	-	-	-	-	-	-	-	-	-
	6/28/2002	-	-	-	-	-	-	-	-	-
	6/12/2003	248.0	249.0	249.0	249.0	249.0	-	-	-	-
	6/20/2003	195.6	195.8	195.9	195.6	195.2	-	-	-	-
	6/27/2003	229.0	230.0	230.0	230.0	230.0	-	-	-	-
	7/10/2007	-	-	-	-	-	-	-	-	-
	9/21/2007	-	-	-	-	-	-	-	-	-
	10/4/2007	-	-	-	-	-	-	-	-	-
	3/12/2008	180.6	180.7	180.6	181.0	180.9	181.6	180.6	201.0	-
	8/29/2010	320.0	319.0	321.0	320.0	319.0	320.0	321.0	320.0	-
	10/6/2010	306.0	305.0	306.0	305.0	306.0	305.0	304.0	305.0	-

Table A5. Maramec Spring measured turbidity.

		Sampling Location								
Measurement	**Date**	**1**	**2**	**3**	**4**	**5**	**6**	**7**	**8**	**Maremec River**
Turbidity (NTU)	3/12/2008	7.53	7.54	7.67	7.53	7.74	8.48	8.24	7.78	4.15
Turbidity Check (6.11 standard)	3/12/2008	6.21	-	-	6.16	6.14	6.10	6.17	6.13	6.15

Table A6. Maramec Spring measured CO_2 flux.

		Sampling Location								
Measurement	**Date**	**1**	**2**	**3**	**4**	**5**	**6**	**7**	**8**	**Maremec River**
CO_2 flux ($\mu moles/m^2 sec$)	8/29/2010	17.50	-	8.50	-	2.60	-	-	-	-

Table A7. Maramec Spring measured calcium hardness, magnesium hardness, total hardness, and alkalinity.

		Sampling Location								
Measurement	**Date**	**1**	**2**	**3**	**4**	**5**	**6**	**7**	**8**	**Maremec River**
Ca Hardness	7/10/2007	101	-	-	-	-	-	-	-	-
(ppm)	10/4/2007	80	90	90	88	80	85	-	-	-
	3/12/2008	54	54	-	-	-	-	-	55	-
	8/29/2010	105	89	84	81	-	-	-	-	-
			-	-	-	-	-	-	-	-
Mg Hardness	7/10/2007	61	-	-	-	-	-	-	-	-
(ppm)	10/4/2007	80	66	72	77	87	73	-	-	-
	3/12/2008	40	39	-	-	-	-	-	35	-
	8/29/2010	50	71	85	83	-	-	-	-	-
			-	-	-	-	-	-	-	-
Total Hardness	7/10/2007	162	-	-	-	-	-	-	-	-
(ppm)	10/4/2007	160	156	162	165	167	158	-	-	-
	3/12/2008	94	93	-	-	-	-	-	90	-
	8/29/2010	156	160	169	163	-	-	-	-	-
			-	-	-	-	-	-	-	-
Alkalinity	7/10/2007	123	-	-	-	-	-	-	-	-
(ppm)	10/4/2007	129	120	125	127	124	123	-	-	-
	3/12/2008	73	70	-	-	-	-	-	74	-
	8/29/2010	144	131	223	149	-	-	-	-	-

Table A8. Maramec Spring water dissolved oxygen measurements.

		Sampling Location								
Measurement	**Date**	**1**	**2**	**3**	**4**	**5**	**6**	**7**	**8**	**Maremec River**
Dissolved	8/29/2010	4.55	4.40	6.68	7.10	7.20	7.80	6.42	7.18	-
Oxygen	10/6/2010	4.04	4.30	6.65	7.84	8.60	8.27	9.00	7.16	-
(mg/l)										

BIBLIOGRAPHY

Anderson, C.B., 2002, Understanding Carbonate Equilibria By Measuring Alkalinity in Experimental and Natural Systems, *Journal of Geoscience Education*, v. 50, n. 4, p. 389 – 403.

Dickinson, S.R., Henderson, G.E., and McGrath, K.M., 2002, Controlling the Kinetic versus Thermodynamic Crystallisation of Calcium Carbonate, *Journal of Crystal Growth*, v. 244, p. 369 – 378.

Dove, P.M. and Hochella, M.F., 1993, Calcite Precipitation Mechanisms and Inhibition by Orthophosphate: In Situ Observations by Scanning Force Microscopy, *Geochimica et Cosmochimica Acta*, v. 57, p. 705 – 714.

Drever, J.L., 2002, *The Geochemistry of Natural Waters: Surface and Groundwater Environments, Third Edition*, Prentice-Hall, New Jersey, 436 p.

Dreybrodt, W., Eisenlohr, L., Madry, B., and Ringer, S., 1997, Precipitation Kinetics of Calcite in the System $CaCO_3$-H_2O-CO_2: The Conversion to CO_2 by the Slow Process of $H^+ + HCO_3^- \rightarrow CO_2 + H_2O$ as a Rate Limiting Step, *Geochimica et Cosmochimica Acta*, v. 61, n. 18, p. 3897 – 3904.

Gebauer, D., Völkel, A., and Cölfen, H., 2008, Stable Pronucleation Calcium Carbonate Clusters, *Science*, v. 322, p. 1819 – 1822.

Gómez-Morales, J., Torrent-Burgués, J., López-Marcipe, A., and Rodríguez-Clemente, R., 1996, Precipitation of Calcium Carbonate from Solutions with Varying Ca^{2+}/carbonate ratios, *Journal of Crystal Growth*, v. 166, p. 1020 – 1026

Gómez-Morales, J., Torrent-Burgués, J., and Rodríguez-Clemente, R., 1996, Nucleation of Calcium Carbonate at Different Initial pH Conditions, *Journal of Crystal Growth*, v. 169, p. 331 – 338.

Goodarz-nia, I. and Motamedi, M., 1980, Kinetics of Calcium Carbonate Crystallization from Aqueous Solutions, *Journal of Crystal Growth*, v. 48, p. 125 – 131

Kamkha, M.A., Sibiryakov, P.B., and Bizyaev, V.L, 1989, Effect of pH on the Kinetics of Mass Crystallization of Calcium Carbonate, *Kinetics and Catalysis*, v. 30, n. 1, p. 62 – 67.

Keller, W.D., Westcott, J.F., and Bledsoe, A.O., 1954, The Origin of Missouri Fire Clays, *in Second National Conference on Clays and Clay Minerals*, Univ. of Missouri, Columbia, Missouri, Oct. 15-17, 1953, Publication #327, p. 7 – 46.

Lakshtanov, L.Z. and Stipp, S.L.S., 2010, Interaction Between Dissolved Silica and Calcium Carbonate: 1. Spontaneous Precipitation of Calcium Carbonate in the Presence of Dissolved Silica, *Geochimica et Cosmochimica Acta*, v. 74, p. 2655 – 2644.

Langmuir, D., 1997, *Aqueous Environmental Geochemistry*, Prentice-Hall, New Jersey, 600 p.

Lebron, I. and Suarez, D.L., 1996, Calcite Nucleation and Precipitation Kinetics As Affected by Dissolved Organic Matter at 25°C and pH > 7.5, *Geochimica et Cosmochimica Acta*, v. 60, n. 15, p. 2765 – 2776.

Nancollas, G.H., 1979, The Growth of Crystals in Solution, *Advances In Colloidal Interface Science*, v. 10, p. 215 – 252.

Nancollas, G.H. and Reddy, M.M., 1971, The Crystallization of Calcium Carbonate: II. Calcite Growth Mechanism, *Journal of Colloid and Interface Science*, v. 37, n. 4, p. 824 – 830.

Ogino, T., Suzuki, T., and Sawada, K., 1990, The Rate and Mechanism Polymorphic Transformation of Calcium Carbonate in Water, *Journal of Crystal Growth*, v. 100, p. 159 – 167.

Orndorff, R. C., Weary, D.J., and Harrison, R.W., 2006, The Role of Sandstone in the Development of an Ozark Karst System, South-central Missouri, *Geological Society of America, Special Paper 404*, p. 31 – 38.

Reddy, M.M. and Gilliard, W.D., 1981, Kinetics of Calcium Carbonate (Calcite)-Seeded Crystallization: Influence of Solid/Solution Ratio on the Reaction Rate Constant, *Journal of Colloid and Interface Science*, v. 80, n. 1, p. 171 – 178.

Reddy, M.M. and Nancollas, G.H., 1971, The Crystallization of Calcium Carbonate I. Isotope Exchange and Kinetics, *Journal of Colloid and Interface Science*, v. 36, n. 2, p. 166 – 172.

Reddy, M.M and Nancollas, G.H., 1973, Calcite Crystal Growth Inhibition by Phosphonates, *Desalination*, v. 12, p. 61 – 73.

Reddy, M.M. and Nancollas, G.H., 1976, The Crystallization of Calcium Carbonate: IV. The Effect of Magnesium, Strontium and Sulfate Ions, *Journal of Crystal Growth*, v. 35, p. 33 – 38.

Söhnel, O. and Mullin, J.W., 1982, Precipitation of Calcium Carbonate, *Journal of Crystal Growth*, v. 60, p. 239 – 250.

Stumm, W. and Morgan, J.J., 1996, *Aquatic Chemistry: Chemical Equilbria and Rates in Natural Waters, 3rd Edition,* John Wiley & Son, New York, 1022 p.

Swinney, L.D., Stevens, J.D., and Peters, R.W., 1982, Calcium Carbonate Crystallization Kinetics, *Industrial & Engineering Chemistry Fundamentals*, v. 21, n. 1, p. 31 – 36.

Teng, H.H., Dove, P.M., and De Yoreo, J.J., 2000, Kinetics of Calcite Growth: Surface Processes and Relationships to Macroscopic Rate Laws, *Geochimica et Cosmochimica Acta*, v. 64, p. 2255 – 2266.

Thompson, T.L., 1991, *Paleozoic Succession in Missouri, Part 2 – Ordovician System*: Missouri Department of Natural Resources, Division of Geology and Land Survey, Report of Investigations 70, part 2, 292 p.

Unklesbay, A.G. and Vineyard, J.D., 1992, *Missouri Geology: Three Billion Years of Volcanoes, Seas, Sediments, and Erosion*, University of Missouri Press, Columbia, 189 p.

Vandike, J.E., 1985, Hydrogeologic Aspects of the November, 1981 Liquid Fertilizer Pipeline Break on Groundwater in the Maramec Spring Recharge Area, Phelps Country, Missouri, *Missouri Speleology*, v. 25, n. 1 – 4, p. 93 – 101.

Vandike, J.E., 1996, *The Hydrology of Maramec Spring*, Water Resources Report No. 55, Missouri Department of Natural Resources, Division of Geology and Land Survey, Water Resources Report No. 55, 104 p.

Wicks, C.M. and Hoke, J.A., 2000, Prediction of the Quality and Quantity of Maramec Spring Water, *Groundwater*, v. 38, n. 2, p. 218 – 225.

Wilson, J.L., 1975, *Carbonate Facies in Geologic History*, Springer-Verlag, Berlin, 471 p.

Zhang, Y. and Grattoni, C.A., 1998, Comment on "Precipitation Kinetics of Calcite in the System $CaCO_3$-H_2O-CO_2: The Conversion to CO_2 by the Slow Process of $H^+ + HCO_3^- \rightarrow CO_2 + H_2O$ as a Rate Limiting Step" by W. Dreybolt, L. Eisenlohr, B. Madry, and S. Ringer, *Geochimica et Cosmochimica Acta,* v. 62, n. 23/24, p. 3789 – 3790.

VITA

Kyle Steven Rybacki was born and raised in the small town of Nashville, Illinois. He has one sibling, Krista, who is following in his geologist boots at the Missouri University of Science and Technology. In May of 2008, Kyle earned a Bachelor of Science degree in Geology and Geophysics from the University of Missouri – Rolla. Kyle graduated Suma Cum Laude with a 4.0 GPA. In December of 2010, Kyle earned a Master's of Science degree in Geology and Geophysics from the Missouri University of Science and Technology.

Kyle is an Eagle Scout and enjoys playing golf, photography, the culinary arts, caving, and spending time with family and friends. He has a border collie, Andesite, who loves field work and travel almost as much as Kyle.

Kyle has worked for the National Park Service as the Guadalupe Mountains National Park's Field Geologist and Speleologist. He is also a member of the MSM Spelunkers and the Cave Research Foundation, which have provided him with opportunities to map caves such as Carlsbad Caverns in New Mexico and Mammoth Cave in Kentucky.